

THE MULTIPHASE HALO OF NGC 891: WIYN H α AND BVI IMAGING¹

J. CHRISTOPHER HOWK² & BLAIR D. SAVAGE

Department of Astronomy, University of Wisconsin-Madison, Madison, WI 53706

Electronic mail: howk@astro.wisc.edu, savage@astro.wisc.edu

Accepted for publication in The Astronomical Journal

ABSTRACT

We present new, deep optical images (BVI+H α) of the interstellar medium (ISM) far above the plane of the edge-on Sb galaxy NGC 891. These sub-arcsecond ($0''.8 - 0''.9$) ground-based images give a direct visual view of two physically distinct “phases” of the thick interstellar disk of this galaxy. A dense, likely cold, phase of the thick disk ISM is observed in our BVI images as highly-structured dust-bearing clouds viewed in absorption against the background stellar light of the galaxy. These dusty structures are traceable to heights $|z| \sim 2$ kpc from the midplane. Though our data are deep enough to identify such clouds at higher z , very few highly-structured dust features are present at $|z| \gtrsim 2$ kpc. If the more prominent dust structures have Galactic gas-to-dust ratios, then they have gas masses in excess of $10^5 M_{\odot}$, each having visual extinctions well in excess of unity. A warm ionized phase of the high- z ISM is observed through its well-studied H α emission. Our images of this medium, to date the highest-resolution observations of the warm ionized medium in NGC 891, show that the diffuse ionized medium in this galaxy is relatively smoothly distributed with some filamentary structure superposed on this smooth background. Our data show very little correspondence between the H α -emitting material and the absorbing dust structures. *These two phases of the multiphase high- z ISM are physically distinct.* The material traced by H α emission is much more smoothly distributed than that traced by the absorbing dust clouds, and it is clear that the H α emission is being heavily extinguished in many places by the dense dust-bearing medium. The high- z dust clouds in NGC 891 are a major component of the multiphase halo medium. The mass found in the cold dense, warm neutral, and warm ionized phases are for $|z| > 0.4$ kpc are comparable and of order a few $\times 10^8 M_{\odot}$. Our discussion of the physics of the multiphase medium at high- z relies heavily on the theoretical work of Wolfire et al., and we suggest the dense phase of the thick disk ISM exists to $|z| \lesssim 2$ kpc because the thermal pressures of the warm and hot phases in this region are sufficient for its maintenance. Our H α observations show evidence for several discrete H II regions at large distances from the midplane ($0.6 \lesssim |z| \lesssim 2.0$ kpc). The presence of these H II regions in the thick disk of NGC 891 suggests that on-going star formation may be present in some of the dense, high- z clouds visible in our images.

Subject headings: dust,extinction – galaxies: individual (NGC 891) – galaxies: ISM – galaxies: spiral – galaxies: structure – ISM: clouds

1. INTRODUCTION

The interstellar medium (ISM) in the disk of the Milky Way (and other spirals) is made up of several thermal “phases,” each with a characteristic density and temperature depending on the prevailing physical conditions (Field, Goldsmith, & Habing 1969; McKee & Ostriker 1977). The principal phases of the neutral material in the disks of spiral galaxies, the cold neutral medium (CNM) and the warm neu-

tral medium (WNM), are expected to exist in rough pressure equilibrium, embedded in the warm and hot ionized phases of the ISM. Under the right conditions, the CNM can include a molecular component from which young stars form.

The conditions in the equilibrium neutral media are dictated by the ambient pressure and the detailed heating and cooling processes in the media (see, e.g., McKee & Ostriker 1977; Wolfire et al. 1995a). This is

¹Based on observations obtained at the WIYN Observatory, a joint facility of the University of Wisconsin-Madison, Indiana University, Yale University, and the National Optical Astronomy Observatories.

²Current address: Dept. of Physics & Astronomy, The Johns Hopkins University, 3400 N. Charles St., Baltimore, MD, 21218; e-mail: howk@pha.jhu.edu.

even the case in the self-gravitating molecular clouds in spirals given the external pressure term in the virial equation (see Elmegreen 1999).

In the “standard” models of thermal phase equilibrium in the neutral media, the most important heating source is the photoejection of electrons from the surfaces of interstellar dust grains (Bakes & Tielens 1994; Wolfire et al. 1995a). Grains are also important as potential coolants (e.g., by recombination of electrons and ions on their surfaces), and in certain conditions may significantly affect the thermal balance of a medium by the removal of heavy elements from the gas-phase. Thus interstellar grains play an important role in the physics of the ISM in the thin gaseous disks of galaxies. Their influence on the thermal state of the gas helps determine the phase structure of the medium, and grains go on to play an important role in the star formation process within the dense ISM.

Our understanding of the physical conditions of neutral clouds in the halos of galaxies is less well developed. From a theoretical standpoint, clouds far from the planes of spiral galaxies should behave similarly to clouds in the disk, with the same heating and cooling mechanisms and possibly similar phase structure (Wolfire et al. 1995a, b). Given the importance of dust grains to the thermal physics of clouds at small heights, z , from the midplane, knowledge of the dust content of high- z material is essential if we are also to understand clouds in the halos and thick disks of spiral galaxies.

Much of the material in the halo and thick disk of a spiral galaxy is thought to originate in the thin interstellar disk. The processes that circulate matter between the thin disks and halos of spiral galaxies operate on both gas *and* dust. However, depending on the method of ejection of matter from the thin interstellar disk and the resiliency of dust grains to destruction by various means (Jones et al. 1994), the dust content of halo material may be different than that of the disk. This can have important implications for the thermal phase structure and physics of high- z gas (Wolfire et al. 1995a,b).

In our own Galaxy there is evidence from gas-phase abundances that individual H I clouds at relatively large distances from the plane contain dust (Sembach & Savage 1996; Savage & Sembach 1996, and references therein). There is also evidence for the existence of dust grains in the thickened warm ionized medium or “Reynolds Layer” of the Galaxy (Howk & Savage 1999a; Lagache et al. 1999, 2000). It would

therefore seem that the processes responsible for lifting the observed gas clouds out of the plane of the Galaxy also affect the dust. And though the dust in the Galactic halo may be to some extent processed, or partially destroyed, the evidence suggests this destruction is not total.

Observations of external galaxies have revealed extensive thickened layers of ionized gas traced by its H α emission in several edge-on spiral systems (e.g., Rand, Kulkarni, & Hester 1990, 1992; Dettmar 1990; Rand 1996; Ferguson, Wyse, & Gallagher 1996; Hoopes, Walterbos, & Rand 1999). These extraplanar layers of so-called diffuse ionized gas (DIG) are thought to be similar to the Reynolds Layer of warm ionized material in the Galaxy (Reynolds 1991). Among the most spectacular examples of extraplanar DIG is seen in the nearby ($D \sim 9.5$ Mpc) edge-on Sb galaxy NGC 891 (Dettmar 1990; Rand et al. 1990; Keppel et al. 1991; Rand 1997, 1998). The observed H α emission from this galaxy implies an ionized gas layer with multiple electron scale-heights of ~ 1.0 and $\sim 2 - 3$ kpc (Hoopes et al. 1999; Rand 1997).³

In Howk & Savage (1997, hereafter Paper I) we initiated a program to study extraplanar dust in edge-on spiral galaxies. We presented high-resolution optical images of the nearby galaxy NGC 891 taken with the WIYN 3.5-m telescope at Kitt Peak National Observatory. These images reveal extensive amounts of highly-structured dust seen in absorption against the background stellar light of the galaxy. The high-resolution WIYN images show hundreds of individual dust-bearing clouds observable to heights $0.4 \lesssim z \lesssim 1.5$ kpc from the midplane along the entire observed length of the galaxy.⁴ A very simple analysis of the radiative transfer suggests these dust structures are relatively opaque ($A_V \gtrsim 0.8$ to 2.0). Assuming gas-to-dust relationships appropriate for the disk of the Milky Way (Bohlin, Savage, & Drake 1978) are applicable to these clouds, the inferred hydrogen column densities were in excess of $N_H \gtrsim 10^{21}$ atoms cm^{-2} , implying quite large masses ($M \gtrsim 10^5$ to $10^6 M_\odot$). Estimates for the potential energies of the observed dusty clouds relative to the midplane are in the range $\Omega \sim 10^{52} - 10^{53}$ ergs, similar to the energy estimates derived for Galactic supershells (Heiles 1979). The implied total gas mass associated with the ensemble of dusty high- z clouds is roughly similar to that estimated for the mass of the extra-

³As we will see below, this galaxy contains an extended dust distribution, with extinction visible to large distances from the midplane. Neither of these studies have accounted for this opacity, which is particularly important for heights $z \lesssim 1.0$ kpc. The dust effects the observed quantity and distribution of emission from gas and stars in the thick disk of NGC 891.

⁴Throughout this work we will use the notation z to denote the distance from the midplane. Unless the value in question refers to a single structure, we will be implicitly assuming $z = |z|$ in our discussion, meaning that the value z refers to distances from the midplane to either side of the galaxy.

planar DIG in NGC 891 ($\sim 10^8 M_{\odot}$; Dettmar 1990). The images presented in Paper I clearly show a substantial amount of dust is present in the thick disk of NGC 891. Subsequent observations by Alton et al. (1998) using the SCUBA submillimeter bolometer have detected $\lambda 850 \mu\text{m}$ emission from extraplanar dust to heights $z \lesssim 2$ kpc in NGC 891. The mere presence of the dust features discussed in Paper I imply that the mechanism(s) responsible for transporting material from the thin interstellar disk into the more extended thick disk of NGC 891 does not destroy the grains. We refer the reader to Paper I for a detailed discussion of the various mechanisms that may be at work in lifting gas and dust out of the thin disks of spirals.

In our second paper of this series (Howk & Savage 1999b, hereafter Paper II), we studied the frequency of such extraplanar dust features in normal spiral galaxies. Based on a small WIYN imaging survey of all the massive, edge-on spirals within $D \lesssim 25$ Mpc observable from the north, Paper II showed that the presence of extraplanar dust is relatively common in normal spiral galaxies, with more than half of the galaxies in our final sample exhibiting prominent extraplanar dust structures. Furthermore, in the galaxies of this survey that had previously been searched for extraplanar DIG, Paper II showed a one-to-one correlation between the presence (or absence) of high- z dust structures and the presence (or absence) of high- z DIG. Thus galaxies showing extended regions of $\text{H}\alpha$ emission far from the plane also showed highly-structured dust clouds visible in our broadband images.

The interpretation of the statistical correlation between the high- z dust structures and the DIG is not clear. In general those galaxies showing high- z dust seemed to be relatively uniform in the properties of the dust-bearing clouds, while the $\text{H}\alpha$ morphologies and brightnesses showed significant variation (see Rand 1996 and Pildis, Schombert, & Bregman 1994). The discussion presented in Paper II argued that the extraplanar dust features seen in these edge-on spirals likely trace a dense phase of the ISM at high- z , separate and physically distinct from the extraplanar DIG. Several lines of evidence were used to argue for such a configuration, though this conclusion was primarily based on the rough column density estimates for the dusty structures and on the general lack of morphological similarity between the dust-bearing and $\text{H}\alpha$ -emitting material. The implied column densities with the observed dimensions of the structures yielded crude estimates of the particle density that were irreconcilable with the expected densities of the extraplanar DIG. The DIG at $z \sim 1$ kpc is expected to have local electron densities of order $n_e \sim 0.2 - 0.3$

assuming a volume filling factor of $f \sim 0.2 - 0.25$ (Rand 1997). The dust features are only detectable in these images because they are significantly denser than their surroundings. Estimates of the particle densities in the extraplanar clouds traced by the dust absorption in the galaxies observed in Paper II are in the range $\sim 1 - 10 \text{ cm}^{-3}$.

While there is now evidence for a statistical relationship between the the presence of extraplanar $\text{H}\alpha$ emission and high- z dust absorption, there is as of yet little information on any physical relationship between the DIG and dust within an individual galaxy. Are these observational tracers measuring the same high- z material, or do they each give insight into a separate phase of the thick disk or halo ISM? In this paper we present much deeper observations of NGC 891 in the BVI bands than the data of Paper I. We also present deep, high-resolution narrow-band ($\text{H}\alpha + [\text{N II}]$) images of ionized gas emission from this galaxy. The purposes of these observations are to probe the known dust structures in this galaxy as far from the midplane as possible, and to directly investigate the physical relationship between the dust features and the DIG in the disk-halo interface of NGC 891.

Our presentation is arranged as follows. In §2 we present a summary of our observations and data processing. This includes a description of our unsharp masking technique. The results of our broadband imaging, and the implications for the extraplanar dust structures, are presented in §3. Our $\text{H}\alpha$ images are discussed in §4, including a direct comparison of the $\text{H}\alpha$ emission from NGC 891 and the morphology of the absorbing dust structures. The implications of the observations, and in particular the comparison of the $\text{H}\alpha$ and dust morphologies, are discussed in §5. That comparison shows that these two observational tracers, the dust absorption and the $\text{H}\alpha$ emission, are revealing two different interstellar phases in the multiphase halo of NGC 891. We summarize the major results of this work in §6.

2. OBSERVATIONS AND REDUCTIONS

2.1. Observations and Processing

All of the observations presented here were obtained with the WIYN 3.5-m telescope at Kitt Peak National Observatory in the fall of 1997, though we have also included some of the data from Paper I in our analysis, which were taken 1996 December 4 (UT). A log of our observations is given in Table 1. This table shows the filter used, the date of observation, and the seeing-limited resolution, expressed as the FWHM (in arcseconds) of Gaussian fits to

the stellar images using the IRAF⁵ routine `IMEXAM`, for each exposure. The images presented here were taken under non-photometric conditions. Our analysis depends only on measures of the relative intensity and does not require photometric calibration (see Paper I).

The WIYN imager in use at the time of our observations is a thinned 2048×2048 STIS CCD with $21 \mu\text{m}$ pixels. Placed at the $f/6.5$ Nasmyth focus of the WIYN telescope, the imager has a $6'.7 \times 6'.7$ field of view, with each pixel subtending $0''.196$ on the sky. The images have been bias-subtracted and flat field-corrected in the usual manner within IRAF.

The flat fields were derived from observations of the ‘‘Great White Spot’’ in the telescope dome. In principle subtle variations in the flat-field of the image could mimic dust absorption in NGC 891 (though very few of the dust features we observe can be referred to as ‘‘subtle’’). Our experience suggests that the dome flats can adequately remove small-scale structures associated with the CCD. In the course of our observing we moved the center of the CCD relative to the galaxy by $2'' - 30''$ with each new exposure. This shifts any instrumental flat field features relative to the galaxy. Each individual image was registered to a common reference frame using the positions of foreground stars. The rms errors in the alignment of the images are typically $\lesssim 5\%$ of a pixel. In the resulting coadded data, the effects of any artifacts associated with the flat field structure of the CCD should be greatly diminished. We have found no real evidence, when comparing our final coadded images with the individual exposures, for confusion of flat-field features with absorbing dust structures.

Table 2 gives the properties of our final coadded images, including the final angular resolution of the images. Each image was smoothed with a Gaussian to the worst resolution in a given band before coaddition. For comparison, at the distance of NGC 891 (~ 9.5 Mpc; Tully 1988), $0''.8$ corresponds to ~ 37 pc. The narrowband images will be described more fully in §2.3. Removal of cosmic rays in the images was performed using standard sigma-clipping algorithms within IRAF. We have derived the astrometric plate solution for our images using a grid of stars whose coordinates were measured in the Digitized Sky Survey. The rms error in using the plate solution to derive coordinates is approximately $1''.0$. The sky background in each frame is estimated by fitting a planar (or in a few cases quadratic) surface to regions of the images free from light of the galaxy. Stars in these regions have been removed using a median smoothing technique. This approach is somewhat problematic given

the galaxy fills such a large fraction of the CCD area. The sky-subtraction is not perfect, but we have endeavored to make as reliable a fit as possible.

2.2. Image Display and Unsharp Mask Procedure

All of the results presented in this work require an effective yet accurate method of displaying our high-quality images. We will rely very heavily on unsharp masked displays of our data to show the multitude of structures present at high- z in NGC 891. Our approach to producing quality unsharp masked displays is discussed in some detail in Paper II, but we present here the principal points of that discussion.

Figure 1 shows our final V-band data for NGC 891, as well as the unsharp masked version of the data. The V-band image (top) is displayed to show the distribution of stellar light along the length of the galaxy. With this display the light from the bulge is saturated, making it difficult to identify high- z dust structures. However, the unsharp mask of the V-band data (bottom) allows us to show the absorbing structures along the entire length of the galaxy in one display. This masked version of the image shows the complexity of the absorbing structures that thread through the bulge area.

We derive the unsharp masked versions of our images by dividing the original image by a version smoothed with a Gaussian kernel having a FWHM of 35 pixels ($6''.9$). With this approach we remove the large-scale gradients in the background light of the galaxy, allowing us to display all parts of the galaxy in a uniform manner. The procedure tends to accentuate structures on scales smaller than smoothing kernel ($\Delta \lesssim 310$ pc at the distance of NGC 891). This can be both an advantage and a disadvantage. Most of the structures we find have minor axis scales similar or smaller than this, though not all. In some sense this offsets the natural tendency to have one’s eye drawn towards very large structures. Although we tend to identify structures only in computer displays of the science images (i.e., not the unsharp masks), the reader’s eye may be drawn more to the small-scale structures in our unsharp masks. As in all of our papers, the unsharp masked images are only used for display, never for quantitative measurements.

Bright stars near NGC 891 can produce large artifacts in unsharp masked images, destroying information over a disproportionately large area. We have produced our unsharp masks by dividing the original data by a smoothed image with such problem stars replaced by a two dimensional fit to the surrounding background light before the smoothing process. The replaced area is usually chosen to be a circular

⁵IRAF is distributed by the National Optical Astronomy Observatories, which is operated by the Association for Research in Astronomy, Inc., under cooperative agreement with the National Science Foundation.

aperture of several times the FWHM of the seeing disk. For fainter examples, the aperture radius was typically twice the size of the seeing disk, while the brighter stars often required apertures in excess of five times the FWHM of the seeing disk. We have also removed the effects of CCD blooming near a few bright stars.

By dividing the original image by the smoothed image with bright stars removed, we are able to keep such stars from influencing large regions of the galaxy, while at the same time showing where these stars lay with respect to the target. Artifacts can be present in our unsharp masked images very near the positions of the brightest stars. Faint halos (white in this display) can be seen around a few of the background galaxies and faint stars in Figure 1.

While there are potential problems associated with the interpretation of the unsharp masks displayed here, this approach is much more effective at showing the reader the true extent and complexity of the dust features we see at high- z in NGC 891. We are confident that, with the exception of some structures visible very near the brightest stars, the dust features seen in our unsharp masked images are real and not artifacts of the masking procedure.

2.3. *Narrowband Emission Line Images*

We will present narrowband images of NGC 891 to study the distribution of ionized gas in this galaxy. To derive an image of the emission lines ($\text{H}\alpha + [\text{N II}]$) from this galaxy, we have taken images through a narrowband filter centered on the $\text{H}\alpha$ emission line, and filters that cover continuum regions on each side of the $\text{H}\alpha$ wavelength region. The characteristics of the on- and off-band filters used are given in Table 3. The filter Off 1 is from the Kitt Peak filter set (KP 809), while the $\text{H}\alpha$ on-band filter and the filter designated Off 2 are from the WIYN filter library (W015 and W016, respectively).

The $\text{H}\alpha$ on-band filter contains emission from the $\text{H}\alpha$ and nearby $[\text{N II}]^6$ lines plus a stellar continuum contribution. To produce a pure emission line image we must subtract off the contribution of the stellar continuum. Our two off-band filters cover wavelength ranges shortward and longward of the $\text{H}\alpha$ emission line. To derive an appropriate continuum image we have coadded the off-band data with an appropriate weighting factor. Each of our off-band images was normalized to one second exposure time and com-

bined with a weighting factor, W , defined as

$$W \equiv [T \times |\lambda_{cen} - \lambda_o|]^{-1}, \quad (1)$$

where T is the average transmission of the filter, λ_{cen} is the transmission-weighted average wavelength of the filter, and λ_o is the rest-wavelength of the $\text{H}\alpha$ emission line. The ratio of the weighting factors for the two off-band filters is $W(\text{Off 1})/W(\text{Off 2}) = 0.81$.

After combining the two off-band filters to produce a single continuum image, we have performed aperture photometry of a grid of ~ 20 stars in the sky-subtracted on- and off-band images. The fluxes derived from these stars were used to determine the relative scaling between the on-band and continuum images. The continuum image was multiplied by this scale factor and subtracted from the on-band image to produce the final emission line image. The use of this scale factor assures that the foreground stars in our image (which should be pure continuum sources) are completely subtracted. Stars which are saturated, however, do not subtract completely.

We reiterate that the size of the galaxy relative to the WIYN imager is large, and our sky subtraction is not perfect. In particular the 5 kpc layer detected by Rand (1997, 1998) cannot be reliably characterized in our images given its extent relative to the size of the CCD. We do detect emission to $z \sim 4$ kpc in our $\text{H}\alpha$ image, but the true amount and distribution of such high- z gas is confused by the background subtraction uncertainties.

2.4. *Dust Feature Nomenclature and Measurements*

Figures 2 through 7 show close-up views of the disk in three sections. Figures 2, 4, and 6 show the unsharp masked views of the central, northeast, and southwest sections of NGC 891, respectively. Each figure shows a $2'7 \times 1'8$ or $7.3 \text{ kpc} \times 4.9 \text{ kpc}$ section of the disk. Figures 3, 5, and 7 show these same sections with several individual dust features identified. Following Paper II we assign each structure an identification of the form NGC 0891:D \pm XXX \pm ZZZ. The ‘‘D’’ denotes a dust cloud. The values XXX and ZZZ are the projected distances (in arcsec) of the features from the center of the galaxy traced along the major and minor axes, respectively. North and east are positive in this reference frame. We assume the center of NGC 891 to be $\alpha_{2000} = 2^h 22^m 33^s.3$, $\delta_{2000} = +42^\circ 20' 52''.5$ (a mean of the de Vaucouleurs et al. 1991 and NED⁷ coordinates⁸) and a position

⁶Our emission line image contains contributions from both $\text{H}\alpha$ and the nearby forbidden $[\text{N II}]$ lines. For brevity’s sake we will hereafter refer to our image as an $\text{H}\alpha$ image, though the reader should be aware that the bandpass also contains the $[\text{N II}]$ transitions.

⁷The NASA/IPAC Extragalactic Database (NED) is operated by the Jet Propulsion Laboratory, California Institute of Technology, under contract with the National Aeronautics and Space Administration.

⁸We found neither individual measurement was in agreement with our images; though the mean matched the optical center of the galaxy in our images quite well.

angle for the disk PA = 23°5 east of north (García-Burillo et al. 1992). The designations are only meant to be approximate, and the equatorial coordinates should be used for making detailed comparisons with other wavebands. Hereafter we will typically abbreviate these identifications $\pm\text{XXX}\pm\text{ZZZ}$.

Table 4 contains the equatorial coordinates, z -heights, and approximate dimensions of each structure identified in Figures 3, 5, and 7. We have roughly outlined each of the identified structures to help the reader identify the regions used in our calculations. In a few cases we mark with dashed lines regions of absorption that may be associated with the identified structure but are not used in our measurements of the structure.

In Paper I we characterized dust structures at high z in NGC 891 by their “apparent extinction,” a_λ . We defined the apparent extinction in a waveband λ as

$$a_\lambda = -2.5 \log(S_{dc,\lambda}/S_{bg,\lambda}), \quad (2)$$

where $S_{dc,\lambda}$ is the surface brightness measured towards a dust cloud, and $S_{bg,\lambda}$ is the surface brightness of the local background (see Paper I). The light measured towards a given dust feature contains an extinguished component of starlight originating behind the feature along the line of sight as well as an unextinguished component emitted in front of the feature. The apparent extinction in a waveband, a_λ , is a lower limit to the true extinction, A_λ , given the unextinguished star light and the unknown contribution of scattering into the beam (see discussion in §3.1). Table 4 contains average values of a_B , a_V , and a_I for each feature (in magnitudes), measured as described in Paper I.

The combined statistical uncertainties and spatial variations in the dust structures give dispersions typically of order 0.05–0.10 mag for the average a_λ values given in Table 4. The systematic errors in the a_B and a_V determinations could be larger. In the B and V images there is significant overlap between the individual dust structures. This overlap often makes the definition of a true continuum or background difficult: at low z the dust so completely covers the galaxy that the definition of a continuum or background for making these measurements is uncertain. Measurements for clouds much below $z \sim 1.0$ kpc can be difficult to make, and the errors on the shorter wavelength apparent extinctions can be great. At larger z , where the dust features become less common and typically show lower a_λ values, the systematic uncertainties are likely less important than the measurement error and spatial variations within an individual cloud. The overlap of the multitude of dust features is less problematic in the I-band, making the a_I measurements more secure than the shorter wavelength apparent extinction values.

3. THE DUSTY THICK DISK OF NGC 891

Our new broadband images reveal a wealth of absorbing structures stretching to very large distances from the midplane of NGC 891. Figure 1 shows our V-band image of NGC 891 and the unsharp masked view of these data. Though we only show the V-band images here, the structure of the dust in the other two wavebands is much the same as that seen in the V-band. The absorbing structures are more prominent in the B-band and less so in the I-band. The V-band images represent a good compromise between the larger opacity at shorter wavelengths and the generally higher signal to noise in the longer wavelength observations.

The primary difference between the current dataset and that presented in Paper I is the depth of the observations. The new broadband data are a factor of ~ 15 , on average, deeper than the data presented in Paper I, though the resolution of the current dataset is slightly worse. This allows us to identify structures against the background stellar light to larger heights from the midplane. We find firm evidence for structures at $z \sim 2.0$ kpc along most of the length of the galaxy. For example, Figure 8 shows a close-up view of the structure identified as $-089 + 039$ in Figure 7, which will be discussed in more detail below. Material that may be associated with this structure can be traced to at least $z \sim 2.0$ kpc, if not higher. Another discrete feature at quite large z is identified as $+033 + 043$ in Figure 3. This structure is seen prominently against the light of a background elliptical galaxy (approximately E0, centered at $\alpha_{2000} = 2^h 22^m 30^s.5$, $\delta_{2000} = +42^\circ 21' 35''.7$) at a height $z \sim 2.0$ kpc. There are a few individual structures that can be identified when examining the one dimensional light distribution at heights as large as $z \sim 2.0 - 2.5$ kpc.

The dust structures are much less prevalent at heights beyond $z \gtrsim 1.8 - 2.0$ kpc than at lower z . Though the background stellar light is rapidly dimming with height, it is clear there are no structures at heights in excess of 2.0 kpc like those seen at heights $z \sim 0.5 - 1.5$ kpc. Our images show the clear signature of the stellar thick disk (see Morrison et al. 1997 and Morrison 1999) in all three wavebands. To confirm the apparent thick disk light in our images was not simply an artifact of the extended wings of the telescope point spread function (PSF), we have fit several bright stars with a Moffat function (Moffat 1969) to approximate the instrumental PSF. We have then constructed several realistic thin disk model light distributions and convolved these with the instrumental PSF. We find at most a few percent of the light observed to heights $z > 3 - 4$

kpc could be the result of scattering of light from the thin disk NGC 891. We have found similar results when including a lower scale-height thick disk than that fit by Morrison et al. (1991), e.g., by adopting scale heights $\lesssim 1$ kpc. Thus there is detected background light against which we could view the dust features to large z -heights (e.g., $z \gtrsim 3$ kpc in the V-band). While a few features can be identified in the range $z \sim 2.0 - 2.5$ kpc, the number of structures at these heights is much less than at lower heights, and the apparent extinctions are very small (typically $a_V \lesssim 0.1 - 0.15$; often unmeasurable in the other two bands).

Color maps of NGC 891 derived from our BVI images give a similar picture: we find NGC 891 gets *bluer* with increasing height until $z \sim 1.9$ kpc or so. The effects of individual dust clouds on the vertical light distribution become significant in one-dimensional cuts through our data at heights in the range $z \sim 1.8 - 2.0$ kpc. This is consistent with a phase change of the material, where dust at heights in excess of this value is more diffusely distributed and hence not visible in our images (see §5). Although, the lack of dust structures at heights beyond $\sim 1.8 - 2.0$ kpc may simply be tracing the maximum extent to which the material was ejected.

We believe the paucity of structures at very high z ($\gtrsim 2.0$ kpc) is a real effect. There is not a large amount of highly-structured (clumped) dust visible in our images at these heights; however, we cannot rule out the existence of a more smoothly distributed component of the dust at very high z . Our images reveal only the dusty structures more opaque than their surroundings. The visible structures are likely tracing significantly denser regions than the surrounding material. The decreasing number counts and apparent extinctions of features at very high z do not imply there is not dust at these heights, but it is clear there are very few of the overdense, dusty clouds seen at low z to be found at heights in excess of $z \gtrsim 2.0$ kpc.

In Paper I we found the number of dust features on either side of the midplane of NGC 891 was roughly similar. This suggests the dust structures do not arise in a warp along the line of sight, which would cause an asymmetry in the distribution of absorbing structures. The present images show that though the number of structures is similar for each side of the midplane, there is an interesting difference in the morphology of the highest- z absorbing structures from one side of the galaxy to the other. The northern side of the galaxy (up in our images) seems to show an extended series of structures oriented roughly parallel to the plane of the galaxy at $z \sim 1.5 - 1.8$ kpc. The structure $-044 + 033$ in Figure 3 is indicative of the dominant orientation of features at these heights. To

the south of the midplane, however, the structures are oriented primarily vertically near $z \sim 1.3 - 1.7$ kpc. These vertically-oriented structures show an open geometry to high z , with a few cometary-like structures (e.g., $-012 - 030$ and $+007 - 032$ in Figure 3). The open structures on the southern side of NGC 891 are possibly tracing galactic outflow or inflow, though other causes may be viable as well.

It is possible that the “flattening” of structures on the northern side of the galaxy is caused by the ram pressure from the motion of NGC 891 through an intragroup medium. The NGC 1023 group to which NGC 891 belongs is dominated, in mass and luminosity, by three disk galaxies (Tully 1980): NGC 1023 (SB0), NGC 891 (Sb/SBb?), and NGC 925 (SBc). The total extent of the group is ~ 1.6 Mpc \times 3.3 Mpc. NGC 891 is 0.78 Mpc projected distance from NGC 1023, similar to the separation between the Milky Way and Andromeda, and 1.5 Mpc from NGC 925. The group as a whole is likely bound (Tully 1980; Hart, Davies, & Johnson 1980), and NGC 891 lies near its periphery. It is not unreasonable to expect that a group composed of three moderately massive disk galaxies with an associated population of dwarf galaxies (at least 10; see Tully 1980) should contain an intragroup medium. The communication of NGC 891’s movement through a hypothetical medium could propagate through the higher- z material to form the horizontally-oriented structures on the northern side of the galaxy.

Other causes for the flattening of the dust structures on the northern side of NGC 891 may be viable as well, such as a slight warp of the disk along the line of sight. However, Swaters, Sancisi, & van der Hulst (1997) have ruled out a prominent line of sight warp in NGC 891 by comparing models with their H I channel maps. Though the morphological differences between the two sides of this galaxy may be interpreted in many ways, the possibility that the flattening of the high- z structures on the northern side is an intriguing possibility.

3.1. *Physical Properties of Individual Dust Structures*

The directly observable physical properties of a subset of dust features are given in Table 4. From these observables we can infer rough information on the column density, mass, and gravitational potential energies of the individual structures. In Paper I the radiation transfer through an individual dust structure was treated very simply. We assumed some fraction x of the stellar light of the galaxy resided between the observer and the dust structure. Therefore, a fraction $(1 - x)$ of the background stellar light was extinguished by the dust feature. In this case the ratio of

the observed surface brightness towards a dust cloud, $S_{dc,\lambda}$, to that of the local background $S_{bg,\lambda}$, could be written

$$S_{dc,\lambda}/S_{bg,\lambda} = x_\lambda + (1 - x_\lambda) \exp[-\tau_\lambda(x_\lambda)], \quad (3)$$

where $\tau_\lambda(x_\lambda)$ is the estimated optical depth in a waveband λ . If x_λ is chosen correctly and scattering is not important, then $\tau_\lambda = \tau_\lambda(x_\lambda)$, where τ_λ is the “true” absorption optical depth. Using observations in three wavebands and assuming x_λ to be constant with wavelength ($x_\lambda = x$), we derived rough corrections to account for the stellar light arising in front of the dust structures. We will denote these corrected values $a_\lambda(x) \equiv 1.086\tau_\lambda(x)$, where we have derived some fraction x of the stellar light to arise in front of the dust structures. The corrected apparent extinctions $a_V(x)$ were derived in Paper I assuming the ratios of the optical depths in the three wavebands followed a Cardelli, Clayton, & Mathis (1989) parameterization of the interstellar extinction curve. The first-order corrected $a_V(x)$ values are lower limits to the true extinction, A_V , given the unknown geometry, and hence the unknown contribution from scattering. The corrected $a_V(x)$ values derived in this way are therefore more correctly called an “attenuation” (e.g., Ferrara et al. 1999; Meurer, Heckman, & Calzetti 1999). If x is roughly correct, we have a relationship $a_V \equiv a_V(0) < a_V(x) < A_V$.

Including the observed values of a_I for the current set of dust features in this approach, however, does not yield a consistent solution for x and $a_V(x)$ for reasonable values of R_V . We believe the reasons for this are (at least) two-fold. The aforementioned differences between the structure of the features when viewed in the B- and V-band data versus that seen in the I-band data imply that the a_λ measurements of individual dust features may be probing different regions of the clouds at different wavelengths. Further, the assumptions made in the very simple approach to the radiation transfer presented in Equation (3) are likely not valid. The effects of scattering may be important. Previously the scattered light could be approximately treated by incorporating it into the value of x . However, it is our belief that the large wavelength range covered by the current set of observations shows the assumed wavelength independence of x is erroneous, at least as formulated in Equation (3).

The values of $a_V \equiv a_V(0)$ given in Table 4 are firm lower limits to the true extinction, A_V , through the individual dust clouds. In Table 5 we show the magnitude of the implied correction by giving $a_V(x)$ for values of $x = 0.0, 0.25, \text{ and } 0.5$. The $a_V(0) \equiv a_V$ measurements are firm lower limits to the true extinction, and we use these in all of our subsequent

calculations.

We can use the lower limits $A_V > a_V(0)$ to roughly estimate several other physically interesting properties of the individual dust features. Assuming the observed relationship between total hydrogen (neutral plus molecular) column density and color excess derived by Bohlin et al. (1978) for the Galactic disk is appropriate for the high- z clouds in NGC 891, we can estimate the hydrogen column density, N_H , of the high- z dust features with:

$$N_H > 1.9 \times 10^{21} a_V(0) [\text{cm}^{-2}] \quad (4)$$

(e.g., Paper II). With an estimate for N_H and the projected surface area of a cloud, we can estimate the enclosed mass in the observed dust structures. The results of these calculations are given in Table 5. The outlines of the dust clouds in Figures 3, 5, and 7 identify the areas used for calculating the mass of each structure. We include a factor of 1.37 correction to the mass estimates for helium and the heavy elements. Assuming rough values for the distribution of mass in NGC 891 we estimate the gravitational potential energy, Ω , of the structures relative to the midplane. We assume the mass is distributed in an isothermal sheet [mass density $\rho \propto \text{sech}^2(z/2z_o)$] with a mass scale height $z_o \sim 0.35$ kpc (e.g., the near infrared observations of Aoki et al. 1991 which roughly agree with the results of Xilouris et al. 1998, who fit exponential disk models to the light distribution) and mass surface density $\rho_o = 0.185 M_\odot \text{pc}^{-3}$ (derived for the solar neighborhood by Bahcall 1984). The potential energies of the structures relative to the midplane are then calculated as in Paper I, using the z -heights and masses from Tables 4 and 5. These estimates are order of magnitude values and should be viewed with some caution.

The values $a_V(0)$ given in Table 5 are in the range 0.2 to 0.8 mag. It is unlikely that the true values of the extinction are anywhere near this small. However, even adopting the smallest allowed values of $a_V(x)$, the estimates of N_H , mass, and energy are still large. These values are derived assuming the gas-to-dust relationships of the Galactic *disk* are appropriate for the high- z structures seen in NGC 891. As discussed in Paper I, the gas-to-dust relationships could be altered by dust destruction in hydrodynamical processes (Jones et al. 1994) or by the separation of the gas and dust through the effects of radiation pressure (Ferrara et al. 1991; Davies et al. 1998). Our images suggest that the destruction of dust grains cannot be too severe, given that high- z dust is visible in any form. Though radiation pressure could play a role in the shaping of the visible dust structures, they are opaque enough to make such a mechanism relatively inefficient.

The column densities given in Table 5 are roughly consistent with $N_{\text{H}} \sim 10^{21} \text{ cm}^{-2}$, or greater. The extinction values and column density estimates suggest that molecular material may be present in these structures (e.g., Savage et al. 1977; see also Elmegreen 1985 and McKee 1989 for theoretical viewpoints). The dust features identified in NGC 891 may contain large amounts of mass, of order $10^5 - 10^6 M_{\odot}$, assuming Galactic gas to dust relationships. The masses are reminiscent of the Galactic giant molecular clouds (GMCs; e.g., Solomon & Sanders 1985). The implied potential energies are also quite large given these masses and large heights above the plane. Sandage (1961) also suggests that the support of an extended, dusty layer of material in NGC 891 must entail large amounts of energy.

It should be pointed out that while detailed radiative transfer models are beyond the scope of this paper, some of the more sophisticated approaches to radiative transfer through a clumpy medium (e.g., Kuchinski et al. 1998; Witt & Gordon 1996) could perhaps help answer some of the more important questions regarding the properties of the observed high- z dust. For example, detailed radiative transfer models might help shed light on the total mass of the dust at high- z and on the effects of high- z dust opacity on optically-derived scale heights (e.g., for determining the scale height of DIG emission).

3.2. Notes on Individual Absorbing Structures

Several of the absorbing structures identified in Figures 3, 5, and 7 warrant further discussion. We briefly comment here on a few of the more spectacular structures visible in our images.

NGC 0891:D $-089 + 039$: As identified in Figure 7 this structure is an individual cloud at $z \sim 1.75$ kpc. However, there are several individual clouds aligned vertically that may make up a seemingly coherent structure traceable from $z \sim 0.2$ to ~ 2.0 kpc. Figure 8 shows a close up view of the unsharp masked V-band image centered on the region around $-089+039$. Several very high- z dust structures can be seen in this region. If $-089 + 039$ represents the upper-most clump of an irregular filament, the low- z anchor is a ring-like structure at $z \sim 270$ pc whose diameter is similar to the width of the filament near its base (~ 210 pc). Our $\text{H}\alpha$ images, which will be discussed below, show an H II region coincident with the inside of the dust ring. The irregular absorbing clump in the center of the dust ring seems to lie in front of the H II region. We find no evidence for $\text{H}\alpha$ emission associated with the filament itself. Like many of the dusty structures seen in our images $-089 + 039$ and the lower- z portions of the filament are seen in absorption against the diffuse $\text{H}\alpha$ emission of the ion-

ized thick disk (see below).

Haffner, Reynolds, & Tufté (1998) have found an ionized filament in the DIG of the Milky Way that seems to stretch to $z \sim 1.2$ kpc as a coherent feature (as evidenced by its velocity structure). However, this filament is *only* seen in $\text{H}\alpha$ emission, with H I, X-ray, and IR emission being absent. The suggested column density is $N_{\text{H}} \sim 10^{19} \text{ cm}^{-2}$, and the stringent limits on the H I column density suggest the structure is almost fully ionized. The Haffner et al. filament therefore has significantly different physical conditions than the extended filament tentatively identified with $-089 + 039$.

If the clouds visible beneath $-089 + 039$ are physically associated, making a coherent, though irregular, filament more than 1.8 kpc in length, it is a uniquely intriguing structure.

NGC 0891:D $-012 - 030$: This structure (identified as feature 7 in Paper I) is clearly cometary shaped with its apex pointed towards the center of the galaxy and a tail of lower column density material extending to high z . We show a close-up of this structure in Figure 9. The center of the head of the cometary structure is at $z \sim 1.3$ kpc, but the trailing material can be traced to almost $z \sim 1.7$ kpc. This structure is exemplary of the vertically-oriented structures at high z on the southern side of NGC 891. We find no evidence for $\text{H}\alpha$ emission associated with this structure.

NGC 0891:D $+122 - 016$ & $+134 - 019$: Together these two structures (identified as features 11a and 11b in Paper I) seem to trace the walls of a supershell centered near $z \sim 800$ pc with a diameter of ~ 600 pc (see Figure 5). As discussed in Paper I and below (§4.3), there is $\text{H}\alpha$ emission loosely associated with the dusty shell walls. The $\text{H}\alpha$ emission from this structure has been discussed also in Pildis et al. (1994). Our images show no “cap” to the structure in the dust distribution, suggesting a supershell open to high z . The $\text{H}\alpha$ images show a patch of diffuse emission at $z \sim 800$ pc that resides near the center of the shell, but this seems not to be the top of the structure, given that the walls traced by the $\text{H}\alpha$ emission can be found to larger z -heights. Perhaps this structure represents a supershell that has experienced “blowout.” We will address this issue in more detail below when we discuss the $\text{H}\alpha$ emission line images.

NGC 0891:D $-010 + 037$: Though this structure is interesting for its height ($z \sim 1.75$ kpc), perhaps its most interesting attribute is that it obscures a background spiral galaxy (see Figure 3). The southern edge of this spiral, centered at $\alpha_{2000} = 2^{\text{h}} 22^{\text{m}} 29^{\text{s}}.6$, $\delta_{2000} = +42^{\circ} 20' 59''.0$, is completely obscured in the B-band. While the V-band shows slightly more of the low- z end of this galaxy, there still appears to be a

significant amount of the galaxy that is simply missing. The analysis of the light from this galaxy could in principle give us a better estimate of the opacity though a high- z dust structure. Unfortunately such an analysis is complicated by the slightly irregular, asymmetric structure of the galaxy. Furthermore, an unresolved source is seen at the apex of the curve traced by the dust structure ($\alpha_{2000} = 2^h 22^m 29^s.7$, $\delta_{2000} = +42^\circ 20' 56''.6$), and directly over the expected emission from the background spiral, in the I-band. This source is not present in either the V- or B-band images. The archival *HST* image presented in Paper I, which is taken through a very broad filter that encompasses much of the V and R bandpasses, clearly shows an unresolved source as well. This object could conceivably be an intermediate age or globular cluster lying behind $-010 + 037$, and hence being extinguished by this dust structure. It is likely not a supernova associated with the background spiral given its relatively constant appearance in images taken over several epochs. If it is a star forming region in the background galaxy, it is much brighter than any other such regions that might exist in the galaxy.

It is clear from visual inspection that this background spiral is very heavily extinguished in the B and V images.

4. THE RELATIONSHIP BETWEEN DUST AND IONIZED GAS IN THE THICK DISK OF NGC 891

4.1. *Extraplanar Diffuse Ionized Gas*

Emission from extraplanar DIG in NGC 891 was first detected by Dettmar (1990) and Rand et al. (1990) through narrowband imaging. Spectroscopic studies of the DIG have more thoroughly characterized its distribution and properties (Dettmar & Shultz 1992; Keppel et al. 1991; Pildis et al. 1994; Rand 1997, 1998).

The DIG layer has been fit by a two-component exponential distribution including a thick disk with an electron scale height $h_z \sim 1$ kpc and a more extended halo with a more uncertain scale height $h_z \sim 2 - 5$ kpc (Hoopes et al. 1999; Rand 1997). It should be noted that these fits have made no correction for the dust that is clearly visible in our broadband images. Fits constrained to match only the light in excess of $z \gtrsim 1.0 - 1.5$ kpc should be reasonably secure. Below $z \sim 1.0$ kpc, the covering factor of the dust features is greater than unity, and below $z \sim 0.5$ there is virtually no information on the intrinsic distribution of optical light from NGC 891.

The power required to ionize the DIG can only be comfortably met by the ionizing radiation from early type stars (e.g., Rand et al. 1990). The strength of forbidden line emission from [N II] and [S II] relative to $H\alpha$ increases with height above the plane

(Dettmar & Shultz 1992; Rand 1997, 1998), as does the strength of [O III] to $H\beta$ (Rand 1998). Pure photoionization models for the DIG (e.g., Sembach et al. 2000; Domgörgen & Mathis 1994) with very dilute ionizing radiation fields can match the high [N II] and [S II] to $H\alpha$ ratios, though the very highest [N II] and [S II] to $H\alpha$ ratios may require heating mechanisms beyond those in low-density ionized nebulae (Reynolds, Haffner, & Tufté 1999). The increase in the [O III]/ $H\beta$ ratio suggests a secondary source of ionization and/or heating may be at work (see discussion in Rand 1998). Given the very high [N II] and [S II] to $H\alpha$ ratios observed in the extraplanar DIG, light scattered from low- z nebulae off of high- z dust grains cannot dominate the observed high- z $H\alpha$ emission (see Ferrara et al. 1996; Wood & Reynolds 1999).

Figure 10 shows our continuum-subtracted $H\alpha$ image of NGC 891. The display in the top panel of Figure 10 shows the faintest diffuse gas, particularly the often faint high- z material, while saturating the brightest emission. The display in the bottom panel is intended to show the structure of only the brightest $H\alpha$, including the very bright structures present above the plane in the northeast section of the disk. We comment briefly here on a few of the important aspects of the emission line images presented in Figure 10. Our primary interest in the $H\alpha$ images is a comparison of the extraplanar DIG and dust morphologies (see §4.3). Thus we will not detail the many aspects of the ionized gas layer (see Dettmar 1990 and Rand et al. 1990 for descriptions of the DIG distribution). However, we will briefly discuss the properties of several individual ionized filaments in §4.2.

Our $H\alpha$ images clearly show emission from the DIG at large distances from the midplane. We detect $H\alpha$ emission to heights exceeding $z \sim 4$ kpc, though our sky subtraction difficulties do not allow us to accurately characterize the highest- z emission. Some of the $H\alpha$ emission is in the form of discrete large-scale filaments, most of which seem to run roughly perpendicular to the midplane. There is also a more diffuse background of $H\alpha$ emission visible along most of the disk and to high z . Several large H II regions on the front side of the galaxy dominate the light near the midplane. As noted by Rand et al. (1990) and Dettmar (1990), there is a strong asymmetry in the strength of the emission between the northeast and southwest sides of the disk (left and right, respectively, in our images); this asymmetry is also seen in the radio continuum observations of Dahlem, Dettmar, & Hummel (1994) and in the far infrared ($50 \mu\text{m}$) observations of Wainscoat, de Jong, & Wesselius (1987). We also see an asymmetry in the light distribution in our broadband images, with

the northeast section of the disk being brighter than the southwest section at most heights $z \lesssim 1.0 - 1.5$ kpc. This appears to be due to a greater amount of intervening high- z absorbing material on the southwest side of NGC 891. The $H\alpha$ asymmetry is much stronger than that seen in the broadband images, and the radio continuum measurements are not affected by dust, implying a real asymmetry in the amount of star formation between the two sides of NGC 891.

Aside from the known extraplanar DIG, we also detect what appear to be several discrete H II regions at high z in NGC 891. These candidate nebulae are visible in Figures 11, 12, and 13 which show the middle, northeast, and southwest sections of the disk, respectively, in $H\alpha$ and dust. These figures will be discussed in more detail below. In Figure 11 an unresolved source in the $H\alpha$ image is seen in the northern side of the disk (in the upper right corner of this display) corresponding to an unresolved continuum source in the broadband images. This object lies at $z \sim 1.3$ kpc above the midplane. A similar object is seen in Figure 12, also on the northern side of the disk (above the disk, near the middle in this display). This object is again coincident with an unresolved source in the broadband images at $z \sim 0.6$ kpc. Several such unresolved knots of $H\alpha$ emission can be seen in Figure 13 at heights $z \sim 900 - 2000$ pc, all of which are coincident with continuum sources. These objects are not among the list of the planetary nebulae identified in NGC 891 by Ciardullo, Jacoby, & Harris (1991). These candidate H II regions and their associated continuum sources will be discussed in a future publication (Howk & Savage, in preparation).

4.2. Large-scale Filamentary Structures in the Ionized Gas

In this section we very briefly summarize the properties of several of the filamentary structures observed atop the more diffuse component of the DIG in NGC 891. We do this both because it allows the reader to compare the general properties and distribution of the ionized gas filaments with those traced by the dust, and because no previous catalog of such structures exists in the literature, though there seems to be a general consensus that this filamentary component is important (Rand 1997, 1998; Rand et al. 1990; Dettmar 1990).

Figure 14 shows another view of our high-resolution $H\alpha$ observations of NGC 891. We have applied an unsharp masking procedure to the $H\alpha$ data displayed in the top panel of Figure 14, while the bottom panel shows the V-band unsharp masked image from Figure 1 for comparison. To produce the unsharp masked $H\alpha$ image shown in Figure 14, we used a Gaussian smoothing kernel with $\text{FWHM} = 35$ pixels ($6''.9$), the

same used in producing the V-band unsharp masked images.

We have identified and labelled a small number of filamentary structures in Figure 14. We summarize the rough properties of the identified filaments in Table 4. These properties include coordinates, z -heights, and dimensions. We use a naming scheme like that adopted for the dust structures in §2.4, identifying each filament using the form NGC 0891:DIG \pm XXX \pm ZZZ. As with our discussion of individual dust structures, our selection of $H\alpha$ -emitting features is biased towards the more spectacular examples at high z (where the confusing influence of dust absorption is lessened).

Figure 14 shows much less small-scale structure in the $H\alpha$ unsharp-masked image than the unsharp-masked images of the V-band data, which accentuate the absorption by dust. In part the smaller number of filaments in the $H\alpha$ images is caused by the sensitivity of our observations to interstellar matter: where the dusty filaments are present in galaxies, they are much easier to observe than the low-intensity $H\alpha$ -emitting filaments. However, it is clear from Figures 10 and 14 that the filamentary structures in the DIG do not show as great a contrast compared with the background emission as the dust structures, which are visible only because they are much more opaque than their surroundings.

Not only are the $H\alpha$ -emitting filaments less numerous (and less prominent) than the dust structures seen in absorption, but much of the $H\alpha$ emission seems to be in the form of a more smoothly-distributed medium. However, the appearance of this “smooth” component is made more complicated by the absorption caused by the dust features seen in our broadband images. We have avoided identifying any apparent structures that may be caused by absorption due to intervening dust.

The distribution of dust-laden filaments is more symmetric about the center of NGC 891 than the distribution of $H\alpha$ filaments. For example, Figure 6 shows the southwest region of the disk contains a number of prominent dust features. Though a few $H\alpha$ -emitting structures seem to be visible in this region most of them are the result of absorption by the irregularly-distributed dust-bearing clouds. The relatively small number of $H\alpha$ filaments in the southwest region of the disk compared with the northeast region is consistent with the general asymmetry in the $H\alpha$ emission across the center of NGC 891 (Rand et al. 1990; Dettmar 1990; Dahlem et al. 1994).

In general the filaments we have identified in Figure 14 are oriented roughly perpendicular to the plane of NGC 891. Most are singular arcs of emitting material, though a few are in the form of shell-like struc-

tures (e.g., NGC 0891:DIG +089 – 034 and the pair +123 – 018 and +133 – 011). The faint ionized structure NGC 0891:DIG +089 – 034 is one of the more spectacular features in our H α image. As identified in Figure 14 (see also Figure 10), it forms a bubble-like structure approximately 650 pc in diameter, centered ~ 1500 pc above the midplane. This structure is closed on itself, and if it traces a superbubble there is no evidence for break-out. However, it is interesting as much for its location above the plane of the galaxy as its morphology. Even single supernova explosions in low-density halos of galaxies can effect their environments on very large scales (e.g., Shelton 1998), and this structure could conceivably be the result of a high- z supernova.

The shell traced out by the pair of filaments NGC 0891:DIG +123 – 018 and +133 – 011, which are associated with the dust structures NGC 0891:D +122 – 016 and +134 – 019, respectively (see below), may also be tracing a large (~ 600 pc diameter) shell in the ISM, though at lower z . This shell, centered at $z \approx 800$ pc, has no obvious “cap” or top, though there is a diffuse patch of emission immediately between these filamentary shell walls. These ionized filaments, along with NGC 0891:DIG +128 + 015 are discussed in some detail by Pildis et al. (1994).

A few of the H α -emitting filaments seem to be more diffuse (thicker) than the typical dust structures (e.g., NGC 0891:DIG +089 – 034 and +026 + 035), though most of those listed in Table 4 are of comparable size to the absorbing dust clouds. The emission measures towards the brightest filaments identified in Table 4 are 2–3 times that of the nearby diffuse component of the H α emission, while the fainter are only 30%–50% brighter. The brightest filaments are only present above the region of vigorous star formation in the NE section of the disk.

There is no evidence in any of our images for absorption that is directly associated with the filaments observed in our H α images. This does not imply these structures lack dust. If we assume that the filaments have emission measures approximately the same as the average at $z \approx 1$ kpc, i.e., $EM \approx 10$ pc cm $^{-6}$ (e.g., Rand et al. 1990), and assume densities of $n_e \approx 0.2$ cm $^{-3}$, then the hydrogen column densities in these filaments should be $N_H \sim 10^{20}$ cm $^{-2}$. If the gas-to-dust ratio in the filaments is similar to gas in the Galactic disk, these structures should not show detectable absorption in our images. We are not sensitive to extinction in the more diffuse component given our method of identifying dust in our images. We discuss in detail the relationship between the observed dust-laden filaments and the morphology of the H α emission in the next subsection.

4.3. The Distribution of Extraplanar Ionized Gas and Dust

The H α images presented in Figure 10 show that the extraplanar DIG in NGC 891 contains many filamentary structures, some stretching to quite large z . However, comparing the H α distribution with that of the dust seen in Figure 1 suggests that the H α -emitting material is more smoothly distributed than the matter traced by the dust absorption. Are these two views of the high- z ISM in NGC 891 tracing the same structures? The answer to this question is almost certainly no. There are very few regions in the thick disk of this galaxy where the DIG and dust structures are associated with one another in our images, and in those few regions the association is only a loose one. There are a large number of regions where the H α emission is obscured by the dust features, usually in much the same amount as the stellar continuum emission seen in our broadband images. Studies of H α emission from NGC 891 must systematically underestimate the ionized gas emission measures at heights $z \lesssim 2$ kpc, though the effect is most important for $z \lesssim 1$ kpc. The extinction due to the dust may also cause the observed distribution of light to differ from the intrinsic distribution; emission scale heights derived from fits to $z \lesssim 1$ kpc may need to be reconsidered given the observed absorption of the H α emission by the dust structures in our images.

Figures 11, 12, and 13 show a comparison of the dust and H α morphology for three regions, one near the center of the galaxy (Figure 11), one 5.5 kpc projected distance northeast of the center (Figure 12), and the last centered 4.4 kpc to the southwest of the center (Figure 13). Each of these figures shows grayscale images of the ionized gas emission as well as the V-band unsharp masked view from a $1'.3 \times 1'.2$ (3.5 kpc \times 3.2 kpc) region of NGC 891 (top and bottom two panels, respectively). In the right two panels, contours of the H α emission are overlaid on top of these grayscale images. The H α contours can be slightly misleading given they show a small number of quantized levels of emission. They do, however, offer a reasonable way of displaying one dataset on top of another. One should use both the grayscales and contours for comparing in detail the distribution of dust and ionized gas and dust in these figures.

It is clear from Figures 11, 12, and 13 that any direct association of the extraplanar ionized gas and dust at high z is very weak. Towards the center of the galaxy, shown in Figure 11, a significant amount of the structure seen in the H α images is simply caused by the absorption of H α photons by foreground dust features. The H α contours are often just offset from the dust features. But the general impression is not one of H α brightening at the edges of the dust fea-

tures, but rather the diminution of the more smoothly distributed background emission. The southwest section of the disk displayed in Figure 13 gives a very similar impression. In particular one can quite clearly see evidence for absorption of $H\alpha$ photons by the low- z portions of the dust structures $-089 + 039$ and $-107 - 020$ (see Figure 7).

One-dimensional cuts of the light distribution of the $H\alpha$ emission reinforce this conclusion that the $H\alpha$ light is being diminished by the absorbing dust structures. Typical measurements of the apparent extinction values towards a number of dust features in our $H\alpha$ images yield results intermediate between the a_V and a_I values. There is typically no increase in the brightness of the $H\alpha$ emission as one nears the location of a dust feature, but rather a diminution of the light from ionized gas.

There are certainly filaments in the $H\alpha$ images that are not simply caused by dust absorption effects, some of which are discussed in the previous subsection. Some of the filaments have also been observed by Rand (1998) to have slightly different forbidden emission line intensities relative to $H\alpha$.⁹ This suggests these structures may be physically distinct from the general background emission and hence not simply the result of dust absorption.

In the northeast section of the disk, shown in Figure 12, we see several dust structures that appear to have been shaped by the effects of star formation (e.g., $+105 - 017$, $+122 - 016$, and $+134 - 019$; see Figure 5). This region of the disk was imaged by Pildis et al. (1994), who described the $H\alpha$ emission from two ionized “supershells.” This side of the disk of NGC 891 is experiencing vigorous star formation as traced by various means (e.g., Rand et al. 1990; Dettmar 1990; Dahlem et al. 1994).

A few of the dust structures in the northeast section of the disk, particularly those with morphologies suggestive of shells and cones, show a loose association of the DIG emission and the dust absorption structures; an association that can likely not be caused by the simple attenuation of background emission. Examining Figure 12 we see the twin walls of a shell traced by the dust structures $+122 - 016$ and $+134 - 019$ on the southern side of the plane (below the plane in this figure). The region immediately interior of the shell walls traced by these dust features is bright in $H\alpha$ emission. However, if one examines the position of the $H\alpha$ contours with respect to the dust absorption, the alignment of the walls traced by the dust absorption and the $H\alpha$ emission is not perfect. In particular the northern-most wall visible in absorption ($+134 - 019$) is not particularly well aligned with the corresponding $H\alpha$ arc, and may even be present

in absorption against the $H\alpha$ emission at high z . Interestingly, though there is an irregular clump of $H\alpha$ -emitting material near the center of this shell, there is little evidence for a top or cap to this shell in the $H\alpha$ images.

Another structure showing a loose association between the $H\alpha$ emitting material and that traced by the dust absorption is the feature identified as $+105 - 017$ in Figure 5. This structure, appearing as a vertical cone open to high- z in the dust absorption, appears to be edge-brightened in $H\alpha$. It is seen just to the right of center, and below the plane, in Figure 12. Both the dust absorption and associated $H\alpha$ emission can be traced to $z \sim 0.8$ kpc from the midplane.

Though a few of the dust structures seen in Figure 12 show evidence for loosely associated $H\alpha$ emission, many of the dust features have no clear-cut association with the extraplanar DIG. Several of the high- z absorbing features seen in Figure 12 seem to be attenuating the $H\alpha$ emission. This attenuation of the $H\alpha$ emission by foreground dust structures is seen along much of the length of the galaxy. The dust is seen to be much more highly clumped than the DIG emission in our images. When viewing our $H\alpha$ images in detail, one is left with the impression that the DIG emission may in fact be quite smooth, with a few filaments within this smooth layer.

All of this discussion regarding an absence of a direct correlation between the observed dust features and the DIG traced by the $H\alpha$ emission does not imply the DIG of NGC 891 is free of dust (see §4.2). In our own Galaxy, there is increasing evidence for dust in the warm ionized medium (Lagache et al. 1999, 2000; Howk & Savage 1999a). However, our broadband absorption detection method would not be sensitive to the expected column densities and smoother structure of the DIG in NGC 891.

5. THE MULTIPHASE HALO OF NGC 891

The deep images presented in this work have shown that $H\alpha$ emission from the extraplanar DIG in NGC 891 is not generally correlated with the dust-bearing clouds seen in absorption against the background stellar light, although there is a very strong statistical correlation between the presence or absence of these two phases of the ISM in spiral galaxies (Paper II). Our observations also show the highly-structured, or clumped, dusty clouds are prevalent only at heights $z \lesssim 2$ kpc from the midplane of NGC 891 while $H\alpha$ emission is seen to much larger z distances. Many of these dust clouds have column densities in excess of 10^{21} cm^{-2} , and enclose masses $> 10^5 M_\odot$. We estimate the *average* densities of these

⁹Rand’s slit for these observations was oriented parallel to the plane at a height $z \approx 700$ pc above the midplane.

high- z clouds are roughly $n_{\text{H}} > 2 - 10 \text{ cm}^{-3}$.

The lack of association between the $\text{H}\alpha$ emission from high- z DIG and the highly-structured dusty clouds seen in our broadband images implies that the $\text{H}\alpha$ emission and the dust absorption are not tracing the same interstellar material. Our images suggest an arrangement of the high- z ISM in NGC 891 where dusty dense clouds, visible through their absorption of the background stellar light, coexist with a more diffuse ionized medium.

We suggest that all of these aspects of the high- z dust features can be understood in the context of a multiphase ISM in the thick disk of NGC 891, possibly in a quasi-stable configuration. The dusty clouds seen far above the disks of spirals likely represent a dense phase of the ISM at high- z . In this case they may be the result of thermal instabilities in the high- z ISM and may perhaps be in pressure equilibrium with either the DIG or hot, X-ray emitting gas (e.g., Wolfire et al. 1995a,b). Our images show the ionized gas is certainly more smoothly distributed than the material traced by the dust clouds. This suggests the volume filling factor of the dense phase is lower than that of the DIG, in accord with theoretical expectations (e.g., McKee & Ostriker 1977). However, given the lack of association between the DIG and the dense material seen in absorption, it is clear that some portion of the warm ionized medium is not associated with cool cores of neutral material, e.g., as envisioned by McKee & Ostriker (1977).

In Paper II the multiphase nature of the ISM in the thick disks of many nearby spiral galaxies was discussed in the context of a quasi-stable configuration of several thermal “phases.” The calculations of the allowable equilibrium thermal states of a multiphase ISM by Wolfire et al. (1995a,b) were used as guidelines for estimating the requisite conditions for such a configuration. These authors calculate detailed thermal and ionization balance of a multiphase medium (see also McKee & Ostriker 1977; Field et al. 1969) and give the results of these calculations for a range of physical conditions of the medium. A minimum pressure requirement must be met to support a stable dense phase of the ISM. In the Wolfire et al. (1995a) models this pressure for high column density clouds ($N_{\text{H}} > 10^{20} \text{ cm}^{-2}$) with conditions appropriate for the disk of the Milky Way is $P^{\text{min}}/k \approx 600 \text{ K cm}^{-3}$. Larger column densities will tend to lower the required pressure, as will a decrease in the ambient radiation field or in the dust to gas ratio relative to those appropriate for the Milky Way disk. Thus the minimum pressure required to support the high- z dust clouds in NGC 891 could be slightly lower than this value.

If we assume the observed structures are cylindri-

cally symmetric, so that their depth along the line of sight is similar to their minor axis lengths, the column density estimates given in Table 5 suggest these structures have densities $\langle n_{\text{H}} \rangle \gtrsim 2 - 10 \text{ cm}^{-3}$. This is much greater than the expected density of the DIG at *any* distance from the plane, further suggesting that the $\text{H}\alpha$ emitting structures are tracing a separate medium than that traced by the dust. This gross density estimate is consistent with the average densities predicted for dense clouds in the Wolfire et al. (1995a) models (see also Paper II).

Our rough calculations in Paper II suggested the average pressures in the DIG or hot ionized medium traced by X-rays were sufficient to support a dense phase of the ISM. For example, the average pressure provided by the DIG is $P^{\text{min}}/k \approx 600 \text{ K cm}^{-3}$ at $z \sim 1.6 \text{ kpc}$ (assuming the electron distribution of Rand 1997 and $T_e \approx 8,000 \text{ K}$). The X-ray emitting gas likely has a larger pressure (Bregman & Houck 1997). The paucity of clouds beyond $z \sim 2 \text{ kpc}$ is understandable in this scenario: at heights in excess of $\sim 2 \text{ kpc}$, the pressure of the ambient medium may be too low to support a dense phase of the ISM. In this case dust may still exist at larger heights above the midplane, but our images are not sensitive to a diffuse component of dust. We are only able to see those regions that are denser (i.e., more opaque) than their surroundings. Given the uncertainties in the distribution, temperature, filling factor, and ionization fraction of the ambient gas, we believe the pressure requirements for confinement of a dense medium are easily met in NGC 891 at heights $z \lesssim 2.0 \text{ kpc}$.

Other theoretical and observational lines of evidence support our conclusion that the dust structures trace a dense medium at high- z . The three-dimensional numerical simulations of gaseous disk dynamics by de Avillez (1999) suggest that the formation of dense interstellar clouds at great z -heights may be a relatively common by-product of the circulation of material between the disk and halo of a galaxy. His simulations follow the temperature, density, and dynamics of parcels of gas in a model galactic disk undergoing star formation, and hence experiencing energy input by supernovae. The combined effects of multiple supernovae produce a fountain-like flow in these models, with gas continually flowing up from the disk and raining down upon it from above. These detailed simulations show cloud formation at high- z . In these simulations the bulk of the clouds are formed between $0.3 \lesssim z \lesssim 1.5 \text{ kpc}$, and de Avillez suggests the formation of dense clouds is much more efficient in regions compressed by shock waves. In particular he finds the intersections of shocks at high- z can serve to compress the gas, which then cools rapidly.

García-Burillo, Combes, & Neri (1999) have observed CO emission from the edge-on galaxy NGC 4013 at high angular resolution ($\sim 3''$). They find about 10% of the emission in their maps comes from high- z material. Our own WIYN images of this galaxy (Paper II) show a high- z dust distribution similar to that seen in NGC 891. Several of the high- z dust features in our images, which have properties similar to those identified in NGC 891 (Howk & Savage 1999c; Paper II) correspond to high- z CO emission in the maps of García-Burillo et al. The direct observation of molecular emission associated with the extraplanar dust structures in NGC 4013 supports our suggestion in Paper II that the high- z absorbing dust structures observed in several edge-on galaxies represent a dense, possibly molecular phase of the thick disk ISM. García-Burillo et al. (1992) and Sofue & Nakai (1993) have also given evidence for a CO-emitting component of the thick disk of NGC 891, though at much lower resolution.

Several candidate H II regions can be identified in our H α images of NGC 891 at heights $z \sim 0.6$ to 2.0 kpc from the midplane (Howk & Savage 1999c; Howk & Savage, in preparation). Associated with these candidate H II regions we find faint continuum sources ($B \sim 22$ to 23 mag). If spectroscopically confirmed, the presence of H II regions at such high- z suggests the underlying stars were formed in the thick interstellar disk of NGC 891. This would require the existence of molecular clouds far from the midplane, and hence lend implicit support to our conclusion that a dense phase of the ISM is present at high- z , visible as the absorbing dust structures seen in our images. These nebulae will also be a useful probe of the physical conditions of the thick disk ISM in NGC 891. For example, our WIYN images constrain the radii of these nebulae to be $r \lesssim 20$ pc. If ionized by B0 or earlier stars, this implies an ambient electron density of at least $n_e \gtrsim 1 \text{ cm}^{-3}$ (Osterbrock 1989). Thus the density of at least one phase of the interstellar thick disk of NGC 891 is quite dense, even at rather large heights above the plane ($z \sim 2$ kpc). Density estimates for the DIG at these heights are factors of 3 – 10 smaller than the lower density limit implied the H II regions, further suggesting large variations in the density of the interstellar thick disk.

We note that the dust filaments seen in our images likely cannot be caused by a gaseous warp in this galaxy, and they are unlikely to be associated with a flare in the outer galaxy. NGC 891 shows no evidence for a warp in its H I distribution (Swaters et al. 1997; Sancisi & Allen 1979), and the relative numbers of the dust features on either side of the midplane are very similar (Paper I), suggesting these features cannot come from a warp along the line of sight. While a

flared gaseous layer cannot be ruled out, it seems unlikely the observed dust features are associated with a flare. At least *some* of the features are clearly associated with regions of vigorous star formation in the disk. The detection of CO from similar extraplanar dust structures in NGC 4013 by García-Burillo et al. (1999) gives some information on the velocities of these structures. In particular, one such dust feature lies immediately above the dynamical center of the galaxy, but is moving at -104 km s^{-1} relative to the systemic velocity of the galaxy. This velocity is clearly incompatible with the location of the structure in a smoothly rotating flared gas layer. Several other features can be identified with velocities inconsistent with their presence in a galactic flare. We do not believe a flared or warped gas layer is causing the dust structures we see in our images.

We believe a self-consistent picture of the high- z ISM in NGC 891 can be drawn in which the thick disk ISM is made up of a multiphase medium, including a cold, dense phase, a warm (neutral and ionized) phase, and a hot phase. The estimated masses of the warm neutral, warm ionized, and cold, dense phases of the ISM above $z \sim 400$ pc are all of order a few $\times 10^8 M_\odot$. The high- z phases of the ISM together represent $\sim 10\%$ of the total mass of the ISM in NGC 891 (Swaters et al. 1997; Dettmar 1990; García-Burillo et al. 1992; Paper I). The mass of the hot ISM at high- z is estimated to be $\sim 4 \times 10^7 M_\odot$ (Bregman & Houck 1997). The presence of the dense phase, in particular, requires a relatively large pressure to large heights above the midplane. The available data on the hot and warm ionized media are consistent with the required pressures in the thick disk of NGC 891.

Such high pressure in this transition region between the thin disk and the more extended halo of the galaxy is required to support the weight of the higher- z gas. However, the origin of this high- z gas, and hence the origin of the high pressure confining the dense clouds, is likely ultimately tied to star formation in the disk of the galaxy. And though the existence of interstellar material in the thick disks and halos of galaxies was once thought to be a relatively rare phenomenon, our previous work (Paper II) implies the transfer of matter from the thin interstellar disks to the more extended halos may be a common property of spiral galaxies. Furthermore, our images imply that this transfer does not destroy the dust grains. This is important since it can therefore be argued that the more extended halos of galaxies may not be completely devoid of dust (see, e.g., Zaritsky 1994).

We have presented deep, high-resolution ground based images of the edge-on spiral NGC 891 obtained with the WIYN 3.5-m telescope. These images were used to study the extensive distribution of extraplanar dust and ionized gas in this galaxy, building on the work presented in Paper I. The major results of our work are as follows.

1. Our deep broadband images show an extensive web of inhomogeneously distributed (clumped) dust far from the midplane of NGC 891. Many of these structures were visible in the images presented in Paper I. These new images presented here show individual absorbing dust structures to heights $z \gtrsim 2.5$ kpc from the midplane. The number and apparent extinctions of these dust structures decreases significantly beyond $z \sim 1.7 - 2.0$ kpc. Structures like those seen at $z \sim 0.5 - 1.0$ kpc would be easily observable to heights $z \sim 3$ kpc if they existed at such heights.
2. We identify a small subset of the high- z absorbing structures and derive their physical properties (see Tables 4 and 5). These structures are characterized by sizes of order 50-300 pc, with optical extinctions exceeding $A_V \sim 0.2 - 0.8$ mag. Assuming Galactic gas to dust relationships the extinction values imply the column density of associated gas in these structures is $N_H \gtrsim 10^{21} \text{ cm}^{-2}$. The implied mass of the associated gas is $M \gtrsim 10^5 M_\odot$ per cloud, and the gravitational potential energies relative to the midplane are large, $\Omega \gtrsim 10^{52}$ ergs. The masses and average extinction values derived for these clouds are reminiscent of the Galactic GMCs, and in general we conclude that the dust structures are tracing the dense cold neutral phase of the high- z ISM.
3. A few of the more spectacular absorbing dust structures are discussed in some detail. These include a cometary structure of width ~ 140 pc and length ~ 500 pc at a height $z \sim 1.3$ kpc from the midplane; a 600-pc diameter supershell centered at $z \sim 0.8$ kpc; and a filament that may stretch from $z \sim 0.2$ to ~ 2.0 kpc.
4. Our deep, high-resolution $H\alpha$ emission line images recover the high- z DIG studied in earlier works (e.g., Rand et al. 1990; Dettmar 1990; Pildis et al. 1994). These data show a filamentary component of extraplanar ionized gas as well as an apparently more diffuse component. In general the DIG emission is much more smoothly distributed than the interstellar

material traced by the dust absorption. The northeast section of NGC 891 shows significantly more emission, both in and out of the plane, than the opposite side of the disk.

5. Though filaments are indeed present in the distribution of the DIG, they are much less numerous and prominent than the filamentary dust-bearing clouds. The excess emission in the filaments is between 30% and 100% the brightness of the background DIG emission. At low z ($\lesssim 1$ kpc) much of the structure seen in the $H\alpha$ images is the result of absorption by the same dust-bearing clouds visible in our broadband images. We identify several ionized, filamentary structures and summarize their rough properties. Our catalog of structures includes a spectacular supershell of diameter ~ 650 pc that is centered ~ 1500 pc above the plane of NGC 891.
6. *A direct comparison of the DIG morphology with that of the complicated extraplanar dust distribution shows little correspondence between the two.* There are many regions where the $H\alpha$ is extinguished by the dust structures in our images, but very few that show a direct physical relationship between these two tracers of high- z material. In the northeast section of the disk, a region showing evidence for very vigorous star formation, there are a few structures that show a loose association between the thick disk DIG and dust. The morphologies of these structures strongly suggest they are connected to the energetic effects of star formation in the underlying disk.
7. The high- z extinction structures seen in our images represent a dense, likely cold, *phase* of the high- z multiphase ISM. This conclusion is based on the lower limits to the dusty cloud extinctions, the mass and density estimates, and the clear separation between the high- z medium traced by the dust structures and that traced by emission from the DIG. Secondary support for this conclusion is provided by the possible existence of star formation, evidenced by several H II regions visible in our $H\alpha$ data, at large distances from the plane; and the recent detection of CO emission from similar dust structures in the galaxy NGC 4013 by García-Burillo et al. (1999). The thermal pressure of the hot and warm ionized gas is sufficient to maintain a stable two-phase neutral medium (warm+cold) at large distances from the plane (Wolfire et al. 1995a), the densest portions of which we are

seeing in our images. The estimated masses of the cold dense, warm neutral, and warm ionized phases at $z > 400$ pc are comparable and of the order a few $\times 10^8 M_{\odot}$.

8. The presence of H II regions, their underlying young stellar populations, and the natal molecular clouds from which these stars have formed in the thick disk of NGC 891 provides an opportunity to study the physics of star formation in an extreme environment. Our broadband images give a direct visual means of studying the dense high- z clouds in this galaxy with superb spatial resolution (for studies of this phase of

the ISM).

It is a pleasure to thank the many people who have made the WIYN telescope a reality. We extend special thanks to those who maintain and operate observatory. JCH recognizes support from a NASA Graduate Student Researcher Fellowship under grant number NGT-5-50121.

This research has made use of the NASA/IPAC Extragalactic Database (NED) which is operated by the Jet Propulsion Laboratory, California Institute of Technology, under contract with the National Aeronautics and Space Administration.

REFERENCES

- Aoki, T.E., Hiromoto, N., Takami, H., & Okamura, S. 1991, PASJ, 43, 755
- Alton, P.B., Bianchi, S., Rand, R.J., Xilouris, E.M., Davies, J.I., & Trewella, M. 1998, ApJ, 507, L125
- de Avillez, M.A. 1999, in The Stromlo Workshop on High-Velocity Clouds, eds. B.K. Gibson & M.E. Putman, in press.
- Bahcall, J.N. 1984, ApJ, 276, 169
- Bakes, E.L.O., & Tielens, A.G.G.M. 1994, ApJ, 427, 822
- Bohlin, R.C., Savage, B.D., & Drake, J.F. 1978, ApJ, 224, 132
- Bregman, J.N., & Houck, J.C. 1997, ApJ, 485, 159
- Cardelli, J.A., Clayton, G.C., & Mathis, J.S. 1989, ApJ, 345, 245
- Ciardullo, R., Jacoby, G.H., Harris, W.E. 1991, ApJ, 383, 487
- Dahlem, M., Dettmar, R.-J., & Hummel, E. 1994, A&A, 290, 384
- Davies, J.I., Alton, P., Bianchi, S., & Trewella, M. 1998, MNRAS, 300, 1006
- Dettmar, R.-J. 1990, A&A, 232, L15
- Dettmar, R.-J., & Schulz, H. 1992, A&A, 254, L25
- de Vaucouleurs, G., de Vaucouleurs, A., Corwin, H.G., Buta, R.J., Paturel, G., & Fouque, P. 1991, *Third Reference Catalogue of Bright Galaxies*, (New York: Springer-Verlag)
- Domgörgen, H. & Mathis, J.S. 1994, ApJ, 428, 647
- Elmegreen, B.G. 1985, in Protostars & Planets II, ed. D. Black & M. Matthews (Tucson: University of Arizona Press), p. 33
- Elmegreen, B.G. 1999, in The Physics and Chemistry of the Interstellar Medium: Proceedings of the 3rd Cologne-Zermatt Symposium, ed. V. Ossenkopf, in press.
- Ferguson, A.M.N., Wyse, R.F.G., & Gallagher, J.S. 1996, AJ, 112, 2567
- Ferrara, A., Bianchi, S., Cimatti, A., & Giovanardi, C. 1999, ApJS, in press.
- Ferrara, A., Bianchi, S., Dettmar, R.-J., & Giovanardi, C. 1996, ApJ, 467, 69
- Ferrara, A., Ferrini, F., Barsella, B., & Franco, J. 1991, ApJ, 381, 137
- Field, G.B., Goldsmith, D.W., & Habing, H.J. 1969, ApJ, 155, L149
- García-Burillo, S., Combes, F., & Neri, R. 1999, A&A, 343, 740
- García-Burillo, S., Guélin, M., Cernicharo, J. & Dahlem, M. 1992, A&A, 266, 21
- Haffner, L.M., Reynolds, R.J., & Tufte, S.L. 1998, ApJ, 501, L83
- Hart, L., Davies, R.D., & Johnson, S.C. 1980, MNRAS, 191, 269
- Heiles, C. 1979, ApJ, 229, 533
- Hoopes, C.G., Walterbos, R.A.M., & Rand, R.J. 1999, ApJ, in press.
- Howk, J.C., & Savage, B.D. 1997, AJ, 114, 2463 (Paper I)
- Howk, J.C., & Savage, B.D. 1999a, ApJ, 517, 746
- Howk, J.C., & Savage, B.D. 1999b, AJ, 117, 2077 (Paper II)
- Howk, J.C., & Savage, B.D. 1999c, in The Physics and Chemistry of the Interstellar Medium: Proceedings of the 3rd Cologne-Zermatt Symposium, ed. V. Ossenkopf, in press.
- Jones, A.P., Tielens, A.G.G.M., Hollenbach, D.J. & McKee, C.F. 1994, ApJ, 433, 797
- Keppel, J.W., Dettmar, R.-J., Gallagher, J.S., & Roberts, M.S. 1991, ApJ, 374, 507
- Kuchinski, L.E., Terndrup, D.M., Gordon, K.D., & Witt, A.N. 1998, AJ, 115, 1438
- Lagache, G., Abergel, A., Boulanger, F., Désert, F. X. & Puget, J.-L. 1999, A&A, 344, 322
- Lagache, G., Haffner, L.M., Reynolds, R.J., & Tufte, S.L. 2000, A&A, in press.
- McKee, C.F. 1989, ApJ, 345, 782
- McKee, C.F. & Ostriker, J.P. 1977, ApJ, 218, 148
- Meurer, G.R., Heckman, T.M., & Calzetti, D. 1999, ApJ, in press.
- Moffat, A.F.J. 1969, A&A, 324, 80
- Morrison, H.L. 1999, in The Third Stromlo Symposium: The Galactic Halo, ASP Conference Series Vol 165, eds. B.K. Gibson, T.S. Axelrod, & M.E. Putman. (San Francisco: ASP), p. 174
- Morrison, H.L., Miller, E.D., Harding, P., Stinebring, D.R., & Boroson, T.A. 1997, AJ, 113, 2061
- Osterbrock, D.E. 1989, *Astrophysics of Gaseous Nebulae and Active Galactic Nuclei* (Mill Valley: University Science Books)
- Pildis, R.A., Bregman, J.N., & Schombert, J.M. 1994, ApJ, 423, 190
- Rand, R.J. 1996, ApJ, 462, 712
- Rand, R.J. 1997, ApJ, 474, 129
- Rand, R.J. 1998, ApJ, 501, 137
- Rand, R.J., Kulkarni, S.R., & Hester, J.J. 1990, ApJ, 352, 1
- Rand, R.J., Kulkarni, S.R., & Hester, J.J. 1992, ApJ, 396, 97
- Reynolds, R.J. 1991, in The Interstellar Disk-Halo Connection in Galaxies; IAU Symp. No. 144, ed. H. Bloemen (Dordrecht: Kluwer), p. 67.
- Reynolds, R.J., Haffner, L.M., & Tufte, S.L. 1999, ApJ, 517, LXX.
- Sancisi, R. & Allen, R.J. 1979, A&A, 74, 73
- Sandage, A. 1961, *The Hubble Atlas of Galaxies*, (Washington: Carnegie Institution of Washington)
- Savage, B.D., & Sembach, K.R. 1996, ARA&A, 34, 279
- Savage, B.D., Drake, J.F., Budich, W. & Bohlin, R.C. 1977, ApJ, 216, 291
- Sembach, K.R., Howk, J.C., Ryans, R.S.I., Keenan, F.P. 2000, ApJ, in press.
- Sembach, K.R., & Savage, B.D. 1996, ApJ, 457, 211
- Shelton, R.L. 1998, ApJ, 504, 785
- Sofue, Y., & Nakai, N. 1993, PASJ, 45, 139
- Solomon, P.M., & Sanders, D.B. 1985, in Protostars & Planets II, ed. D. Black & M. Matthews (Tucson: University of Arizona Press), p. 59
- Swaters, R.A., Sancisi, R., & van der Hulst, J.M. 1997, ApJ, 491, 140
- Tully, R.B. 1980, ApJ, 237, 390
- Tully, R.B. 1988, *Nearby Galaxies Catalog* (Cambridge: Cambridge Univ. Press)
- Wainscoat, R.J., de Jong, T., Wesselius, P.R. 1987, A&A, 181, 225
- Witt, A.N., & Gordon, K.D. 1996, ApJ, 463, 681
- Wolfire, M.G., Hollenbach, D., McKee, C.F., Tielens, A.G.G.M., & Bakes, E.L.O. 1995a, ApJ, 443, 152

- Wolfire, M.G., McKee, C.F., Hollenbach, D., & Tielens, A.G.G.M. 1995b, ApJ, 453, 673
- Wood, K., & Reynolds, R. 1999, ApJ, in press.
- Xilouris, E.M., Alton, P.B., Davies, J.I., Kylafis, N.D., Papamastorakis, J., & Trewhella, M. 1998, A&A, 331, 894
- Zaritsky, D. 1994, AJ, 108, 1619

TABLE 1
LOG OF OBSERVATIONS

Filter	Date [UT]	Exposure [sec]	Seeing [arcsec]
Broadband Observations			
B	1997 August 30	1200	0.8
B	1997 August 30	900	0.6
B	1997 August 30	900	0.7
B	1997 August 31	1200	0.8
B	1997 August 31	1200	0.8
V	1996 December 04	120	0.7
V	1997 August 30	1200	0.7
V	1997 August 30	1200	0.8
V	1997 August 31	900	0.6
I	1997 August 30	840	0.7
I	1997 August 30	1500	0.7
I	1997 August 31	1200	0.7
I	1997 November 28	820	0.8
Narrowband Observations			
H α	1997 August 31	1200	0.7
H α	1997 August 31	300	0.8
H α	1997 November 26	1800	0.6
H α	1997 November 26	1800	0.6
H α	1997 November 26	1800	0.6
H α	1997 November 26	1800	0.7
H α	1997 November 29	1200	0.6
H α	1997 November 29	1800	0.8
H α	1997 November 29	1200	0.8
H α	1997 November 29	1200	0.7
Off 1	1997 November 26	1800	0.6
Off 1	1997 November 26	1800	0.6
Off 1	1997 November 29	1200	0.8
Off 2	1997 August 30	1200	0.9
Off 2	1997 August 31	900	0.7

TABLE 2
FINAL DATASET

Filter	Exposure [sec]	Seeing [arcsec]
B	5400	0.77
V	3420	0.80
I	4360	0.81
H α	14100	0.77 ^a
H α Off	6900	0.90

^aThough the on-band H α data have a resolution of 0''.77, we have smoothed these data to match the 0''.9 resolution of the off-band data to produce the final H α image.

TABLE 3
NARROW BAND FILTER CHARACTERISTICS

Filter	λ_{cen} [Å]	FWHM [Å]
H α (W015)	6570	73
Off 1(KP809)	6488	67
Off 2(W016)	6618	72

TABLE 4
OBSERVED PROPERTIES OF INDIVIDUAL HIGH- z DUST FEATURES

ID ^a [NGC 0891:D]	R.A. [J2000]	Dec. [J2000]	$ z $ ^b [pc]	Dimensions [pc \times pc]	a_B ^c [mag.]	a_V ^c [mag.]	a_I ^c [mag.]	Morphology
-119 - 019	02 22 30.8	+42 18 55	870	270 \times 75	0.37	0.22	0.15	Flaring Cloud
-107 - 020	02 22 31.2	+42 19 06	880	200 \times 100	0.50	0.35	0.19	Irr. Cloud
-089 + 039	02 22 26.9	+42 19 45	1750	300 \times 160	0.28	0.25	0.19	Irr. Cloud
-044 + 033 ^d	02 22 29.1	+42 20 23	1450	100 \times 50	0.77	0.56	0.30	Elongated Cloud
-012 - 030 ^e	02 22 35.2	+42 20 29	1300	140 \times 60 ^f	0.36	0.32	0.17	Cometary Cloud
-010 + 037	02 22 29.8	+42 20 57	1660	240 \times 120	0.32	0.21	0.16	Arc
+007 - 032	02 22 36.2	+42 20 47	1430	110 \times 90 ^f	0.27	0.24	0.13	Cometary Cloud
+017 + 016 ^g	02 22 32.5	+42 21 14	730	350 \times 75	1.02	0.83	0.49	Column
+033 + 043	02 22 30.8	+42 21 40	1950	200 \times 55	... ^h	... ^g	... ^h	Irr. Cloud

TABLE 4—*Continued*

ID ^a [NGC 0891:D]	R.A. [J2000]	Dec. [J2000]	$ z ^b$ [pc]	Dimensions [pc×pc]	a_B^c [mag.]	a_V^c [mag.]	a_I^c [mag.]	Morphology
+105 – 017 ⁱ	02 22 39.0	+42 22 34	750	700 × 290	0.50	0.40	0.27	Vertical Cone
+122 – 016 ^j	02 22 38.9	+42 22 39	730	270 × 60	0.63	0.56	0.31	Shell Wall
+134 – 019 ^k	02 22 39.6	+42 22 50	845	400 × 50	0.40	0.35	0.23	Shell Wall

^a Identification of the feature using the nomenclature NGC 0891:D ±XXX±ZZZ (see text). We only list ±XXX±ZZZ in the main body of the table.

^b Projected height above the midplane, or the limit to which very extended features can be traced.

^c Average apparent extinction for the BVI wavebands in magnitudes, as defined in the text.

^d Identified as feature 2 in Paper I.

^e Identified as feature 7 in Paper I.

^f The size of the head of these cometary structures is listed. The overall extent of each, including the potential tail material, is ~ 500 pc for $-012 - 030$ and ~ 200 pc for $+007 - 032$.

^g Identified as feature 4 in Paper I.

^h This feature lies in front of a background elliptical galaxy, making its properties difficult to measure.

ⁱ Identified as feature 10 in Paper I.

^j Identified as feature 11a in Paper I.

^k Identified as feature 11b in Paper I.

TABLE 5
DERIVED PROPERTIES OF INDIVIDUAL HIGH- z DUST FEATURES

ID ^a [NGC 0891:D]	$a_V(x)$ [mag.] ^b			N_H^c [cm ⁻²]	Mass ^d [M _⊙]	Energy ^e [ergs s ⁻¹]
	$x = 0$	$x = 0.25$	$x = 0.5$			
-119 - 016	0.22	0.30	0.50	$> 4 \times 10^{20}$	$> 1 \times 10^5$	$> 9 \times 10^{51}$
-107 - 017	0.35	0.50	0.87	$> 7 \times 10^{20}$	$> 9 \times 10^4$	$> 6 \times 10^{51}$
-089 + 039	0.25	0.35	0.58	$> 5 \times 10^{20}$	$> 3 \times 10^5$	$> 6 \times 10^{52}$
-044 + 032	0.56	0.84	1.79	$> 1 \times 10^{21}$	$> 1 \times 10^5$	$> 2 \times 10^{52}$
-012 - 030	0.32	0.45	0.78	$> 6 \times 10^{20}$	$> 1 \times 10^5$	$> 2 \times 10^{52}$
-010 + 037	0.21	0.29	0.47	$> 4 \times 10^{20}$	$> 2 \times 10^5$	$> 3 \times 10^{52}$
+007 - 032	0.24	0.33	0.55	$> 5 \times 10^{20}$	$> 4 \times 10^4$	$> 6 \times 10^{51}$
+017 + 016	0.83	1.35	...	$> 2 \times 10^{21}$	$> 6 \times 10^5$	$> 3 \times 10^{52}$
+105 - 017	0.40	0.57	1.04	$> 8 \times 10^{20}$	$> 9 \times 10^5$	$> 4 \times 10^{52}$
+122 - 016	0.56	0.84	1.78	$> 1 \times 10^{21}$	$> 5 \times 10^5$	$> 3 \times 10^{52}$
+134 - 019	0.35	0.50	0.87	$> 7 \times 10^{20}$	$> 3 \times 10^5$	$> 2 \times 10^{52}$

^aIdentification of the feature using the nomenclature NGC 0891:D \pm XXX \pm ZZZ, where XXX is the distance in arcsec from the optical center of the galaxy traced along the major axis, and ZZZ is the distance in arcsec from the optical center of the galaxy traced along the minor axis (see text). We only list \pm XXX \pm ZZZ in the main body of the table.

^bLower limits to the V-band extinction assuming a fraction x of the stellar light resides in front of the dust feature, given for $x = 0, 0.25,$ and 0.5 . The listed values $a_V(x)$ are lower limits to the true extinction, A_V , due to our neglect of scattering into the line of sight.

^cApproximate lower limit to the column density of material assuming $N_H > 1.9 \times 10^{20} a_V(x = 0)$ cm⁻² (see text).

^dApproximate mass based upon the estimated column density and projected area. Includes a factor of 1.37 correction for He.

^eRough estimates for the potential energy of each structure relative to the midplane using the projected distance from the midplane and the estimated mass (see text).

TABLE 4
OBSERVED PROPERTIES OF INDIVIDUAL DIG FILAMENTS

ID ^a [NGC 0891:DIG]	R.A. [J2000]	Dec. [J2000]	$ z ^b$ [pc]	Dimensions [pc×pc]
+026 + 035	02 22 31	+42 21 30	1570	750 × 150
+089 − 034 ^c	02 22 39	+42 22 02	1510	600 × 180
+111 + 024	02 22 35	+42 22 45	1100	700 × 130
+123 − 018 ^d	02 22 39	+42 22 40	820	500 × 100
+128 + 015 ^e	02 22 36	+42 22 58	660	400 × 60
+133 − 011 ^d	02 22 39	+42 22 52	510	270 × 90
+149 − 022	02 22 40	+42 23 02	1010	700 × 50

^a Identification of the H α -emitting filament using the nomenclature NGC 0891:DIG \pm XXX \pm ZZZ (see text). We only list \pm XXX \pm ZZZ in the main body of the table.

^b Projected height above the midplane, or the limit to which very extended features can be traced.

^c This structure is in fact a large shell. The height and position listed in the table are appropriate for the center of the shell. The dimensions are appropriate for the thickness and rough vertical length of the shell walls. The shell itself is \sim 650 pc in diameter.

^d This filament is associated with the shell formed by the dust structures NGC 0891:D +122 − 016 and +134 − 019. Together they make up one of the “supershells” discussed by Pildis et al. 1994.

^e This structure is part of one of the “supershells” discussed by Pildis et al. 1994. In our higher resolution image it is not clear that this structure truly represents a supershell.

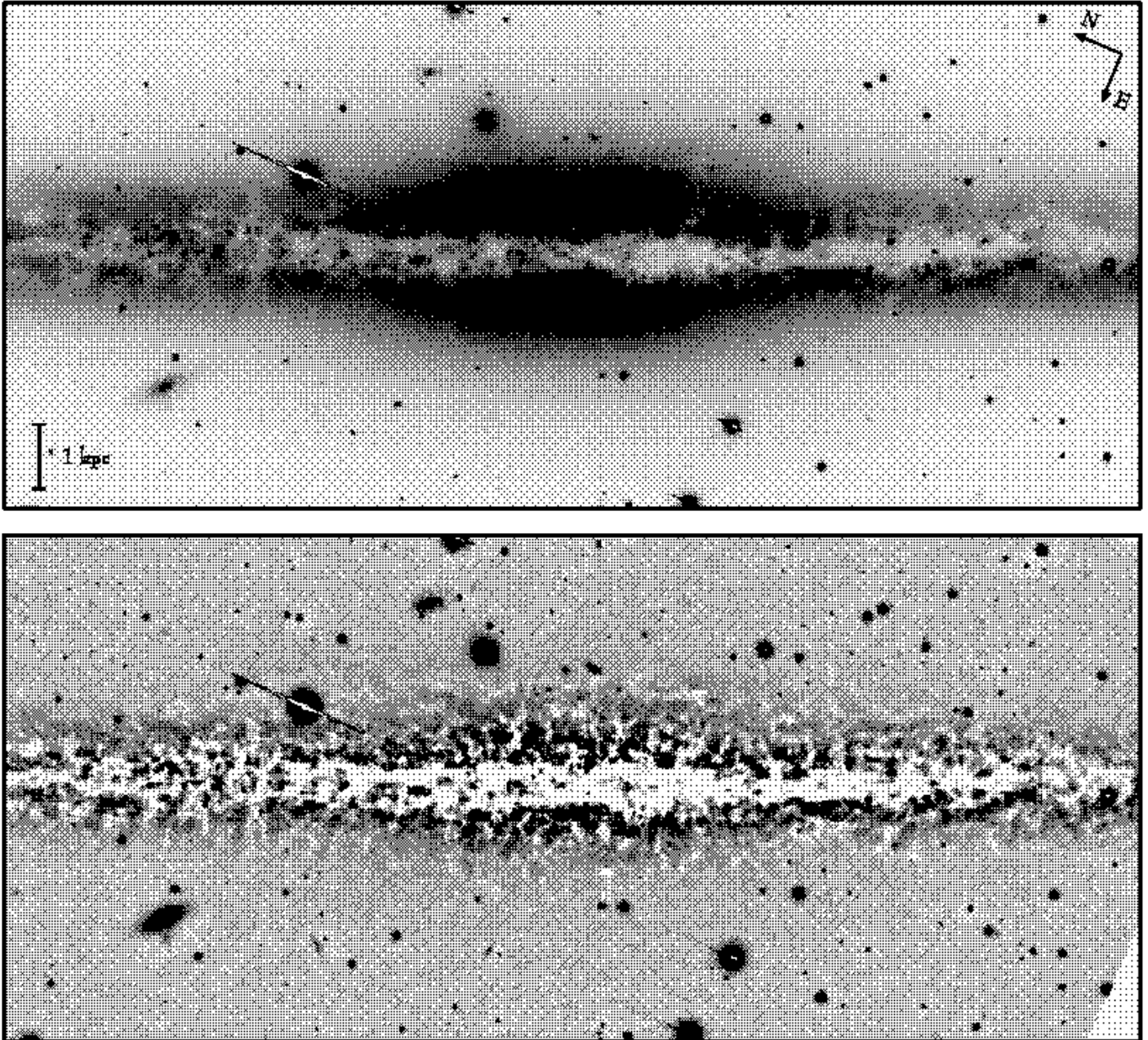


FIG. 1.— WIYN V-band images of NGC 891. The top panel shows the V-band image, while the bottom panel shows the unsharp masked version of this image. The display is inverted such that darker regions represent brighter emission. Regions of dust extinction are lighter than their surroundings. This image covers $6'.4 \times 2'.8$ ($17.3 \text{ kpc} \times 7.6 \text{ kpc}$); a scale bar denoting 1 kpc is shown. North and east are marked. Note that this display is flipped across the y -axis from the figures in Paper I (e.g., Figure 2 of Paper I) to be consistent with most other published images. The dust absorbing structures provide a direct view of the dense neutral medium in the multiphase halo of NGC 891.

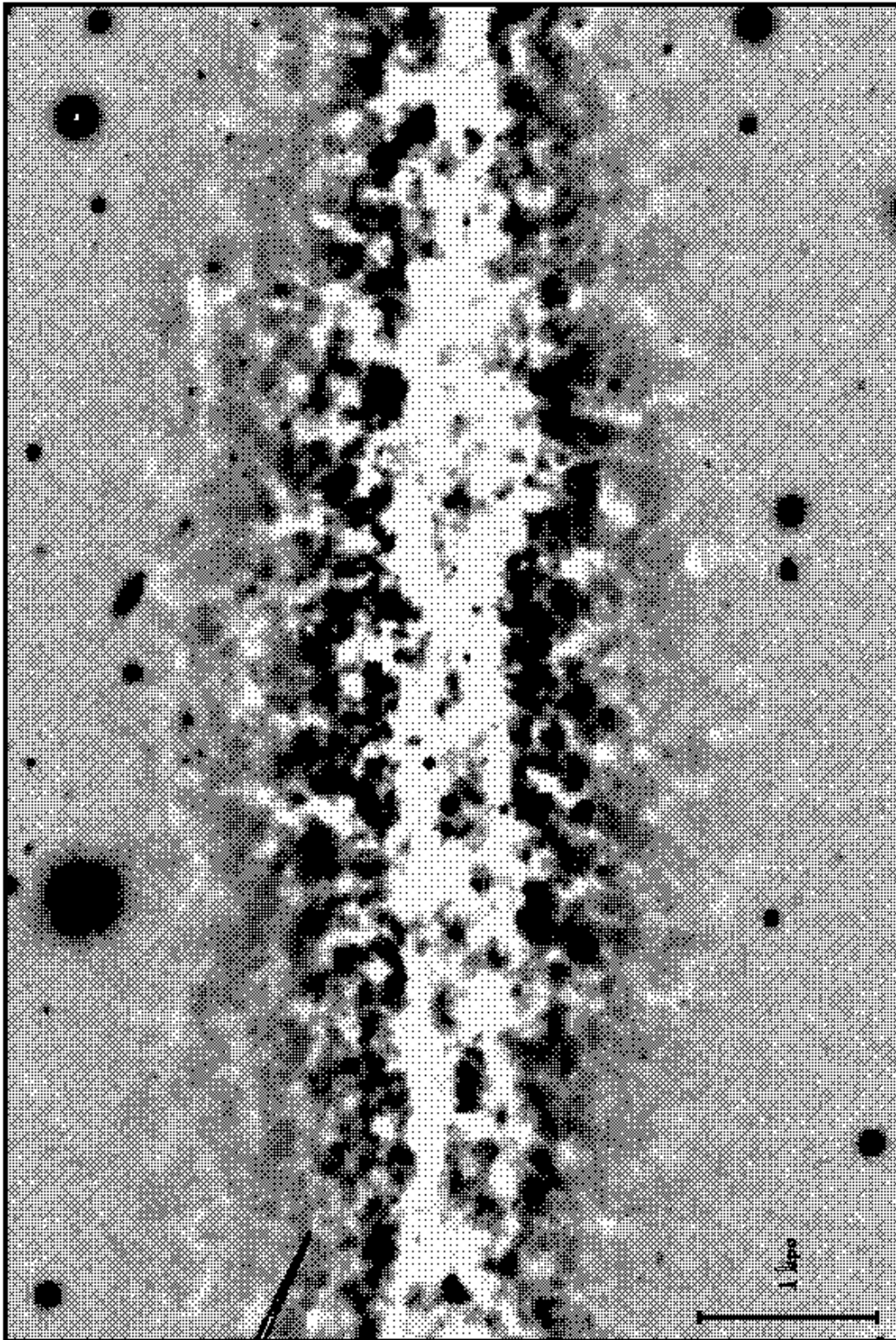


FIG. 2.— An expanded view of the unsharp masked V-band data for a section of the central $2'.7 \times 1'.8$ (or $7.3 \text{ kpc} \times 4.9 \text{ kpc}$) of NGC 891. A 1 kpc scale bar is displayed in the lower left corner of the image.

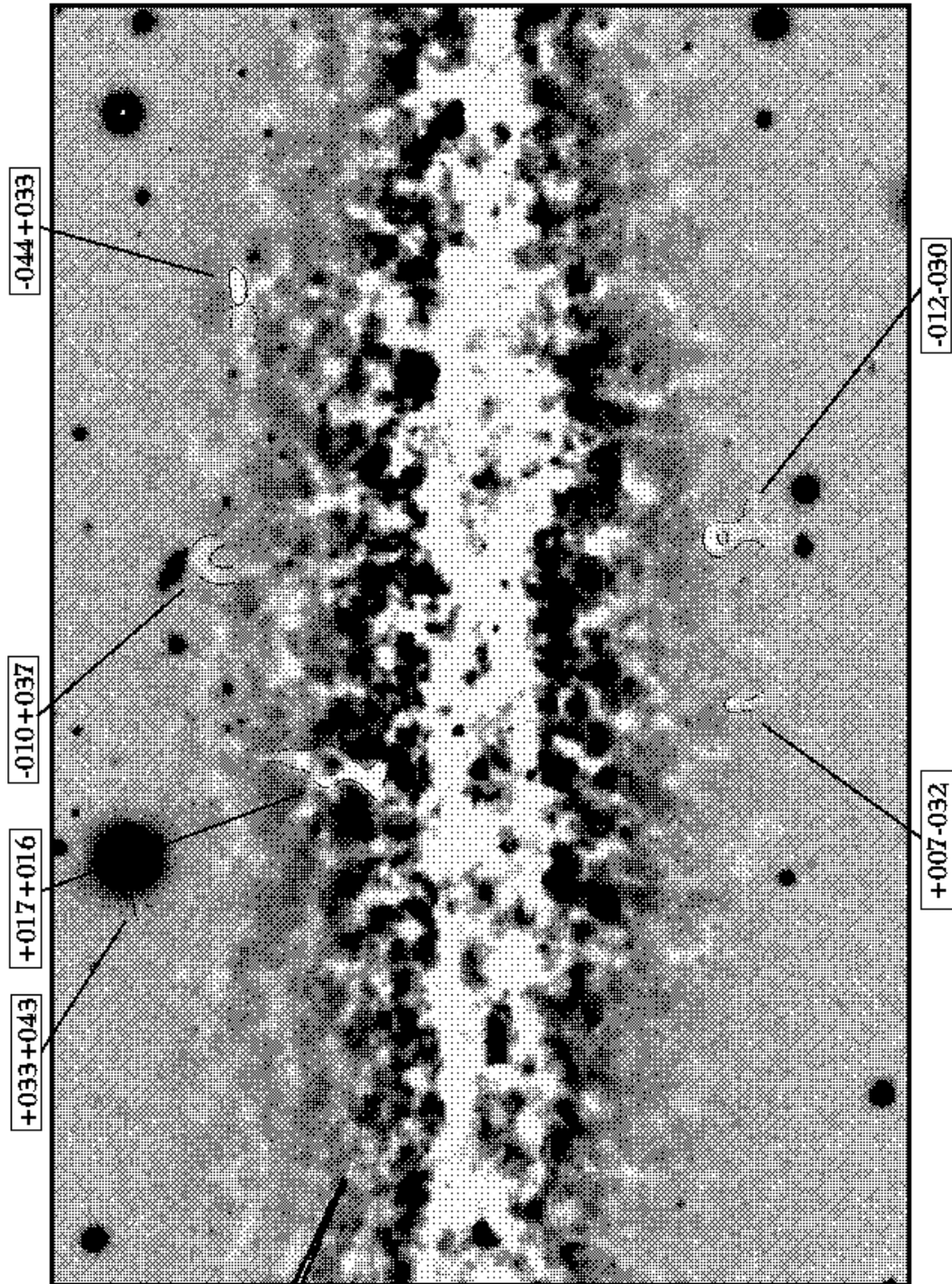


FIG. 3.— The same region as Figure 2, but with several individual absorbing structures identified. The properties of these clouds are summarized in Tables 4 and 5.

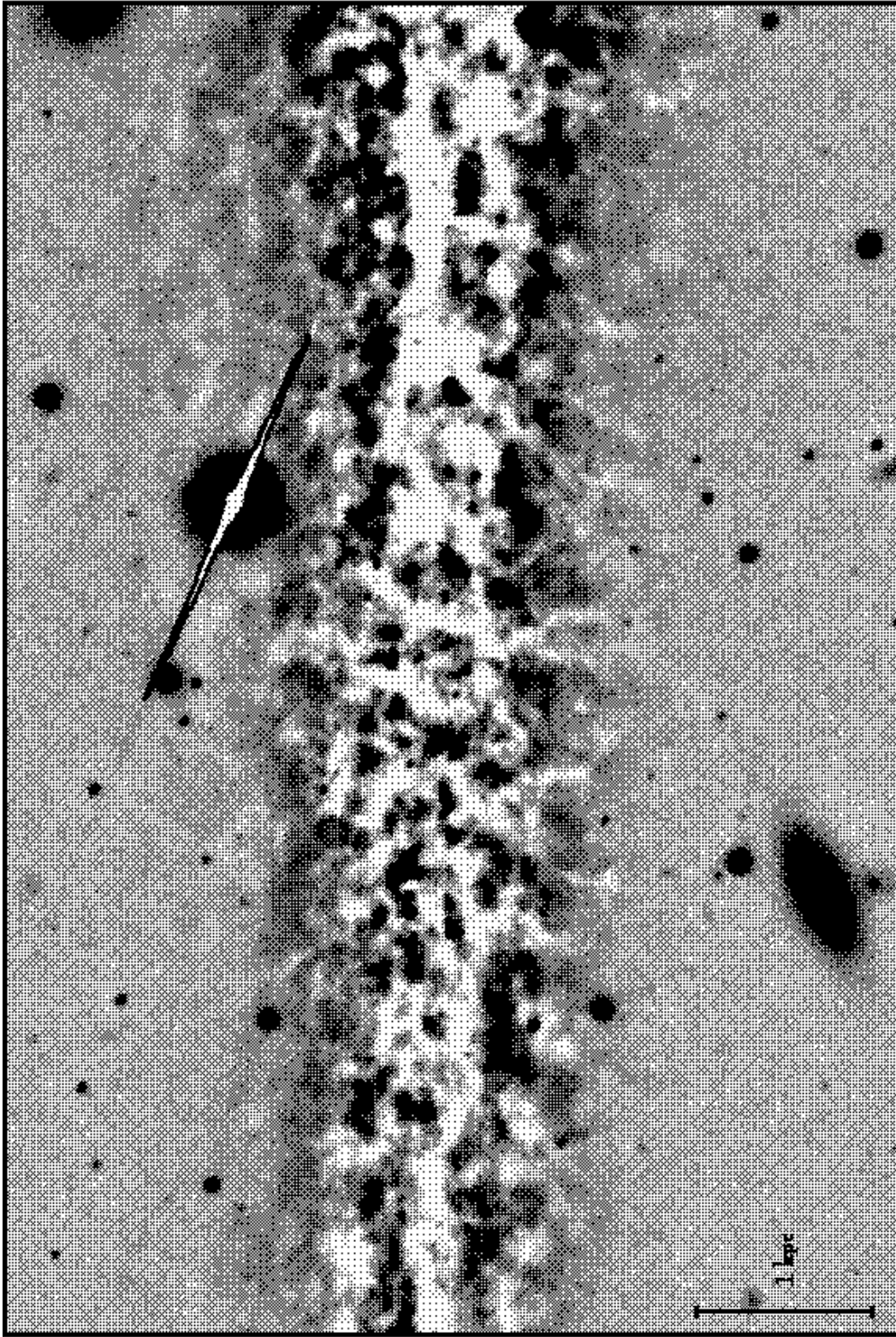


FIG. 4.— As Figure 2 but showing a section of the disk of NGC 891 centered to the northeast of the nucleus.

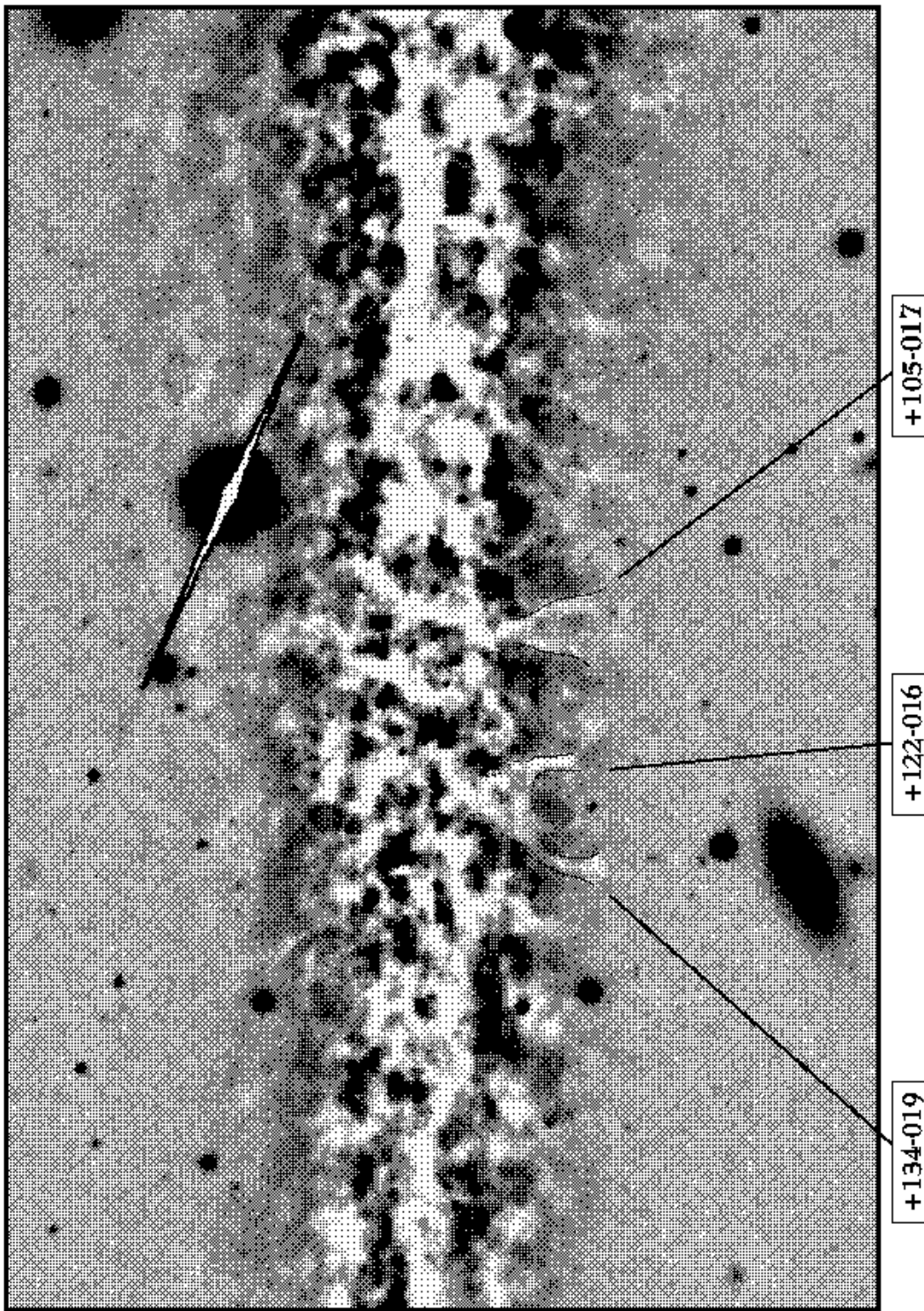


FIG. 5.— The same region as Figure 4, but with several individual absorbing structures identified. The properties of these clouds are summarized in Tables 4 and 5.

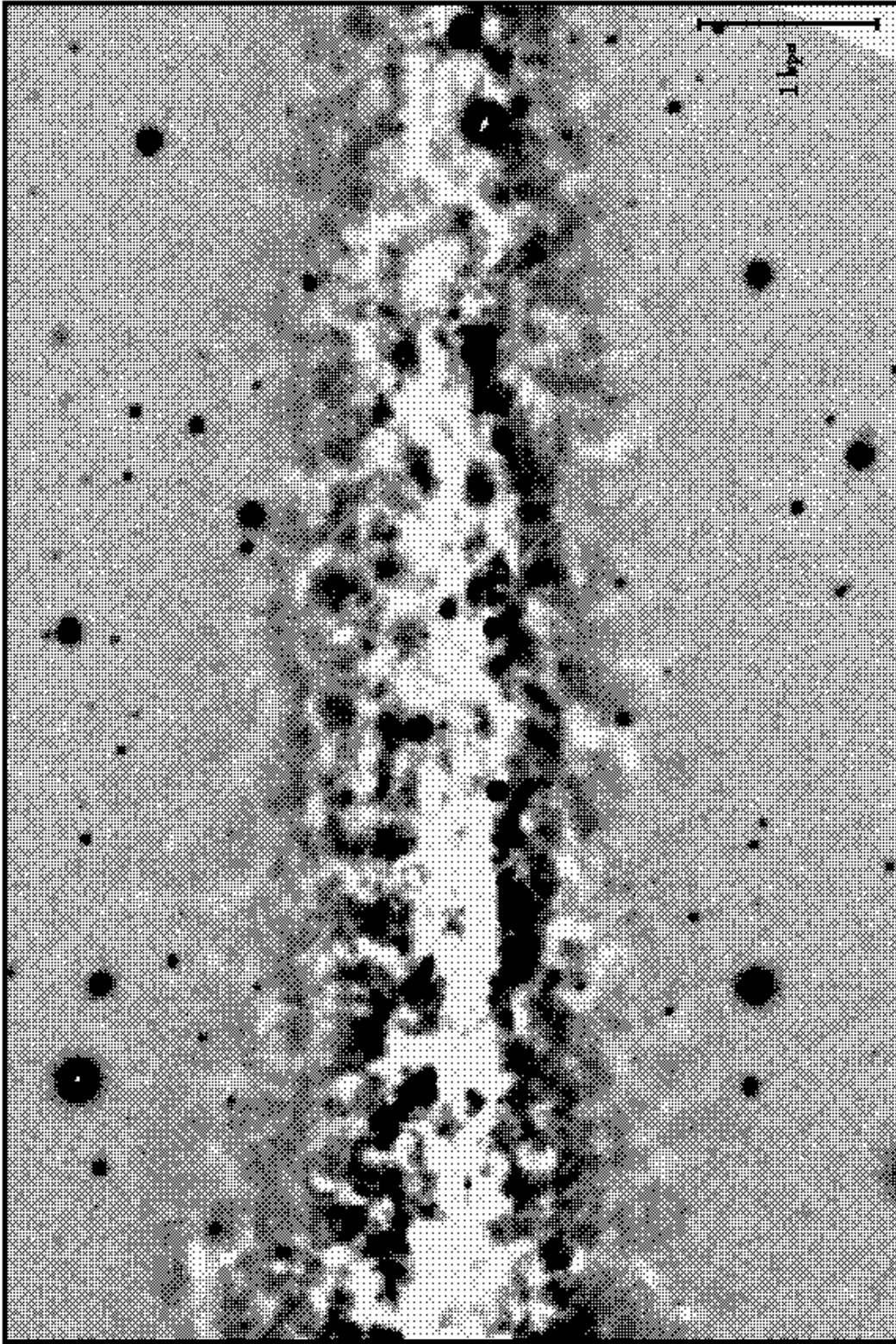


FIG. 6.— As Figure 2 but showing a portion of the disk to the southwest of the nucleus.

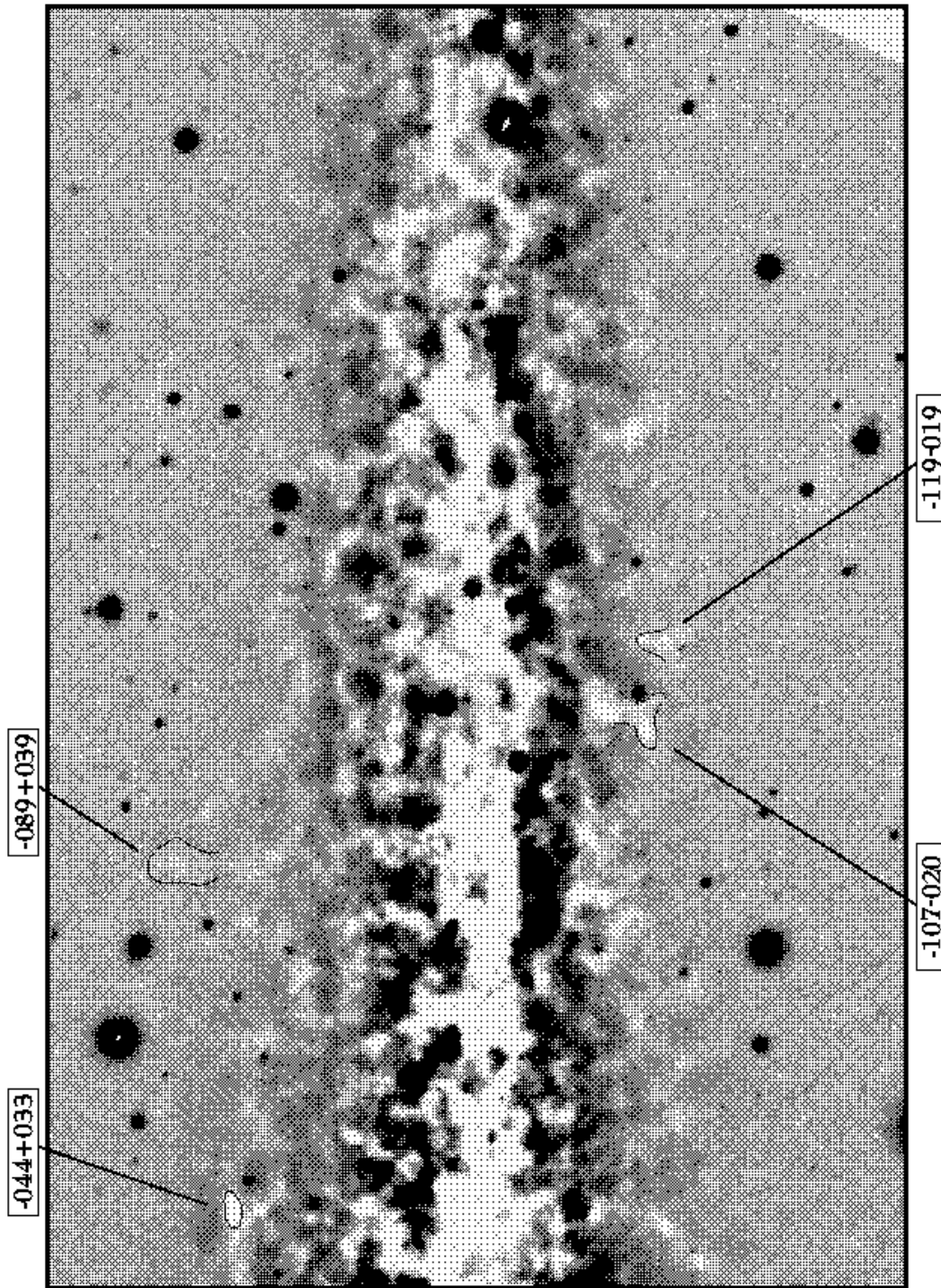


FIG. 7.— The same region as Figure 6, but with several individual absorbing structures identified. The properties of these clouds are summarized in Tables 4 and 5.

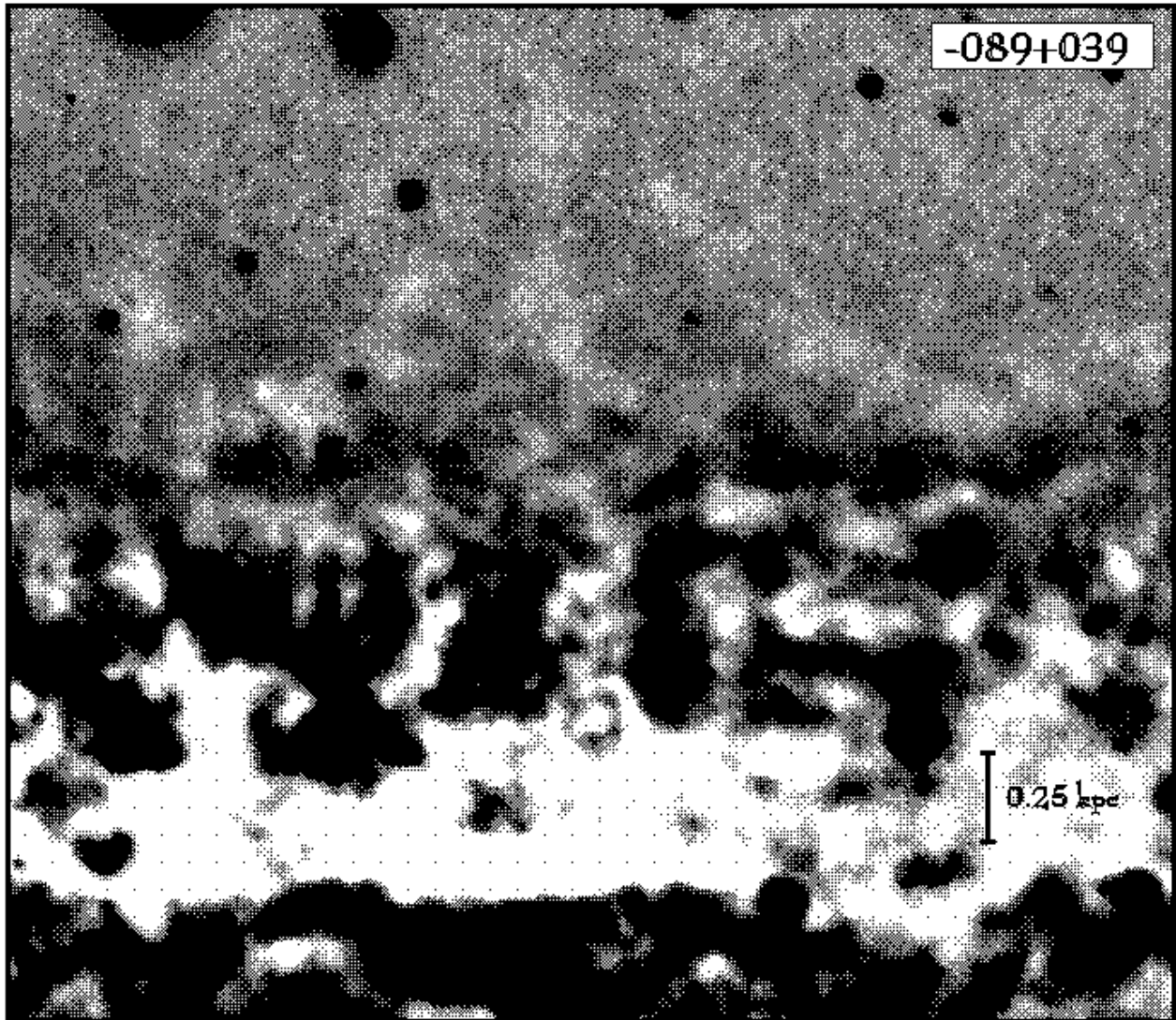


FIG. 8.— A close-up view of the unsharp masked V-band data showing NGC 0891:D -089+039. This structure as identified in Figure 7 is only the top-most cloud centered at $z \sim 1850$ pc. However, this cloud may be part of a much larger structure traceable almost to the midplane. Absorption from material aligned with this structure can be traced to $z \sim 2.0$ kpc, and possibly higher. A scale bar of 0.25 kpc length is shown.

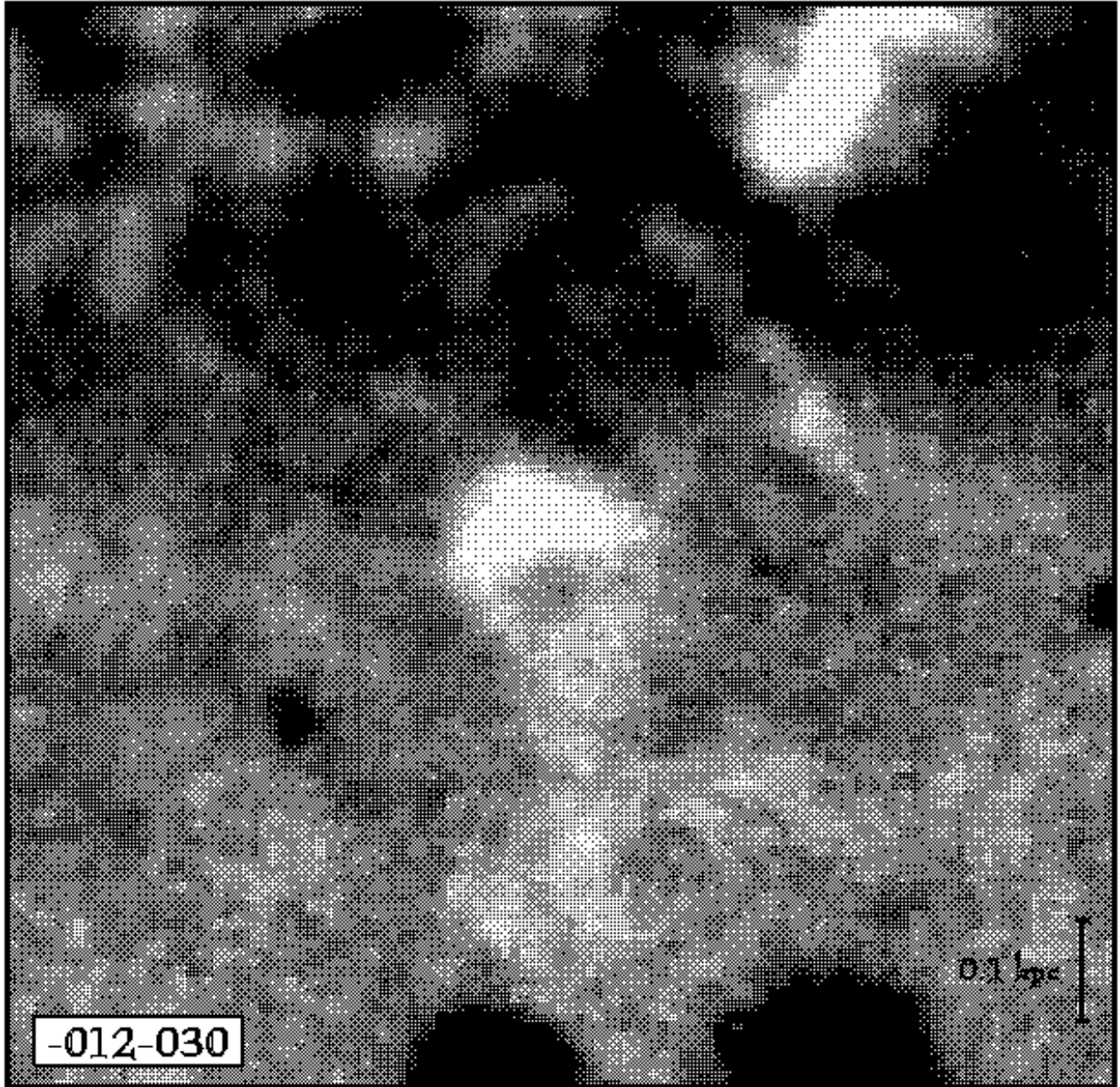


FIG. 9.— A close-up view of the unsharp masked V-band data showing NGC 0891:D -012 - 030. This structure is a cometary-shaped cloud with lower column density absorption trailing to high z . Only the “head” or low- z component of this is described by the data presented in Tables 4 and 5. The 140×60 pc head of this structure lies at a distance $z \sim 1.3$ kpc from the midplane, though the trailing absorption can be traced for an additional ~ 400 pc. The section of the image shown here is $2'$ (or 1.08 kpc) on a side. A scale bar of 0.1 kpc length is given.

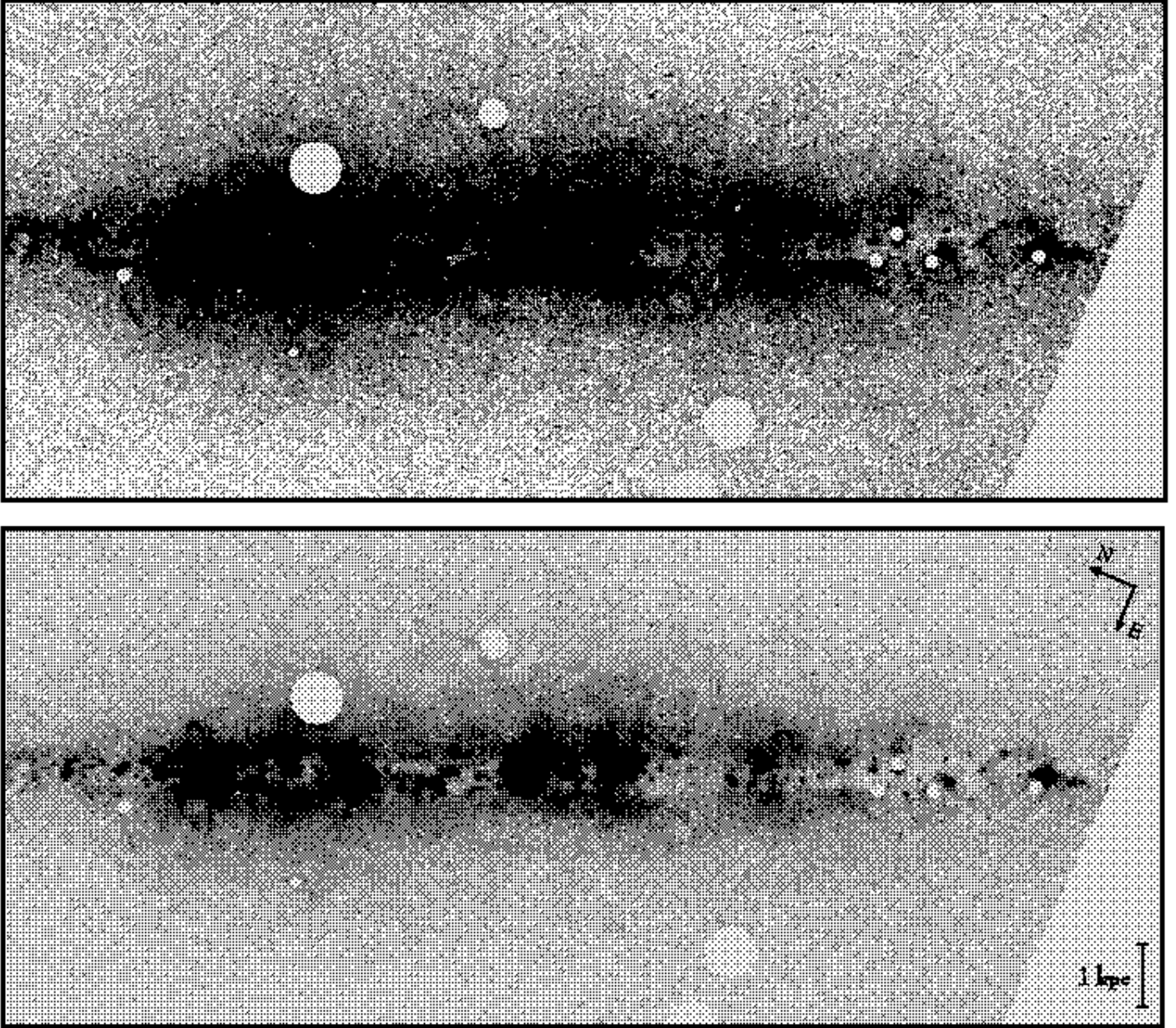


FIG. 10.— The continuum-subtracted $H\alpha$ emission line image of NGC 891. The image is displayed in the top panel to show the faintest diffuse gas, while the display in the bottom panel shows the distribution of bright $H\alpha$ emission. These images cover the same area, $6'.4 \times 2'.8$ ($17.3 \text{ kpc} \times 7.6 \text{ kpc}$), and have the same orientation as those shown in Figure 1. A bar denoting 1 kpc is given for scale in the lower right hand corner of the lower panel. We have placed gray circles over regions where the halo of the point spread function from bright stars in our on-band images may contaminate the view of the ionized gas emission. Note that the $H\alpha$ emission is much less structured than the dust absorption illustrated in Figures 1–9.

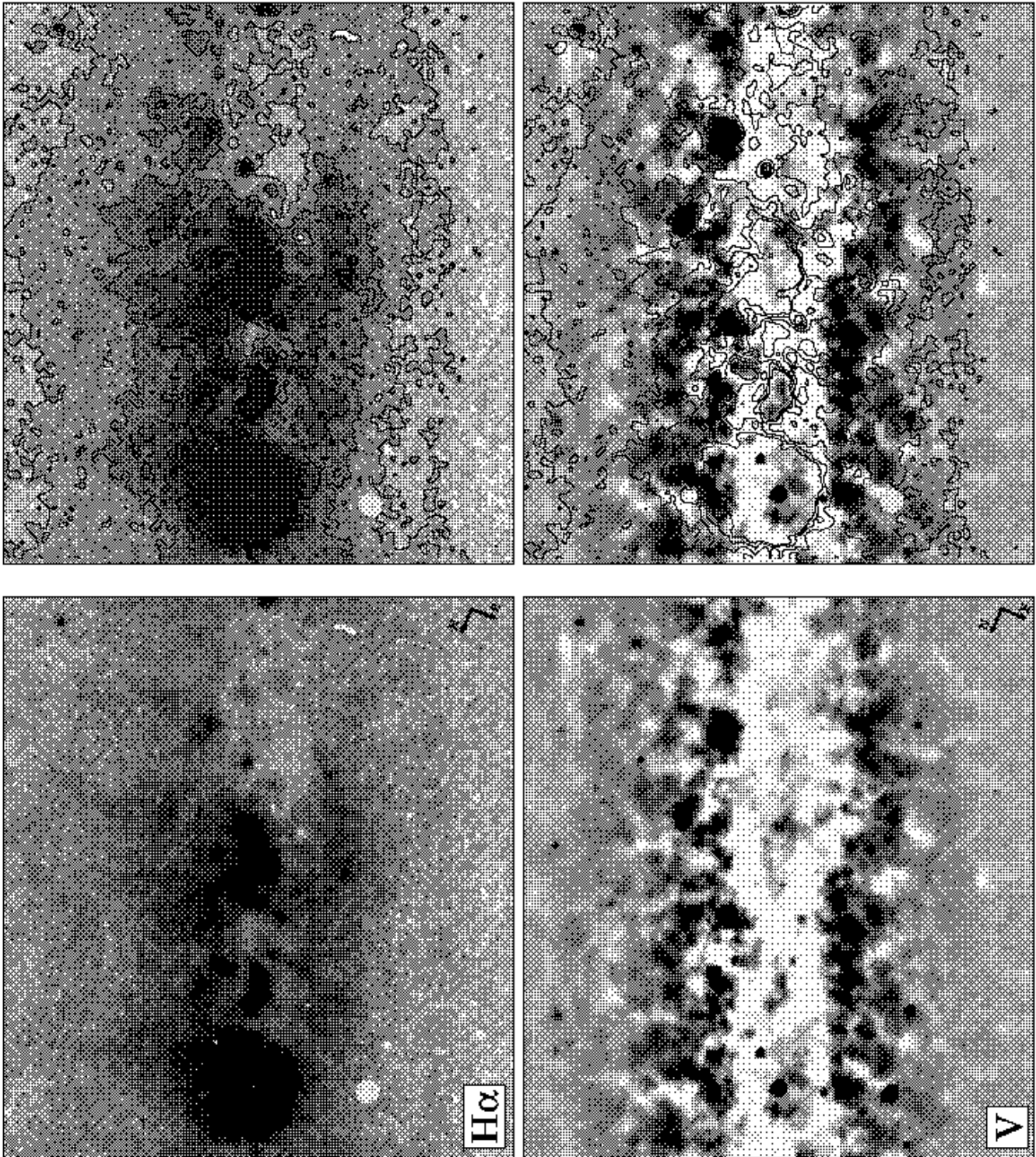


FIG. 11.— A comparison of the $H\alpha$ emission and dust absorption near the center of NGC 891. The continuum-subtracted $H\alpha$ and V-band unsharp masked data for this region are shown as grayscale in the upper and lower panels, respectively. The two right hand panels have $H\alpha$ contours overlaid on the grayscale images. The $H\alpha$ grayscale is shown using a logarithmic stretch. The $H\alpha$ contours are approximately 5σ , 10σ , 15σ , 20σ , and 25σ above the background. The region shown in this image covers $1'3 \times 1'2$ ($3.5 \text{ kpc} \times 3.2 \text{ kpc}$) and is centered $\sim 0.5 \text{ kpc}$ southwest of the galaxy center. Small bright white spots in the $H\alpha$ grayscale are due to the effects of poorly removed cosmic rays in the off-band images.

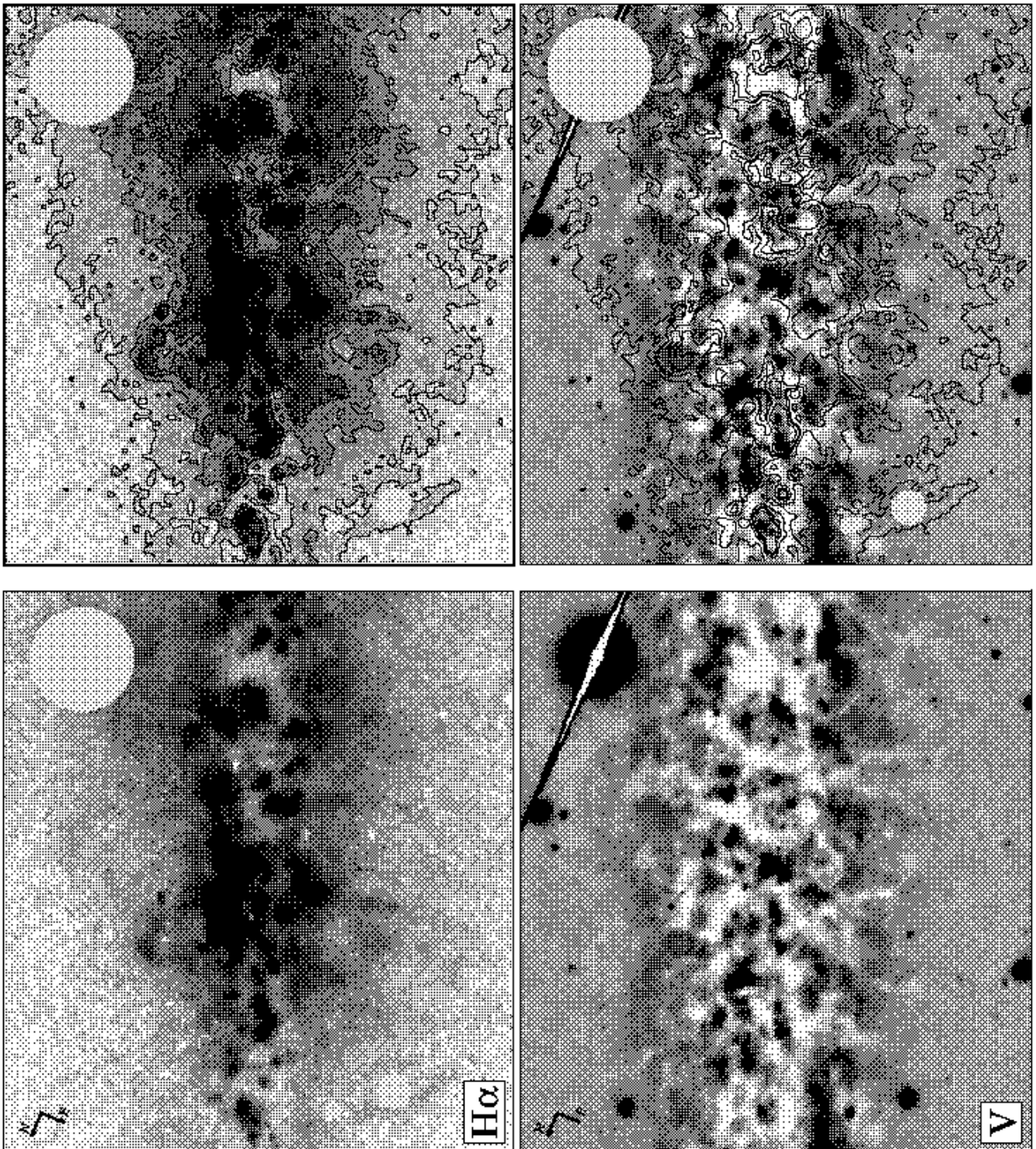


FIG. 12.— As Figure 11 but for a section of the disk centered ~ 5.5 kpc northeast of the nucleus of NGC 891.

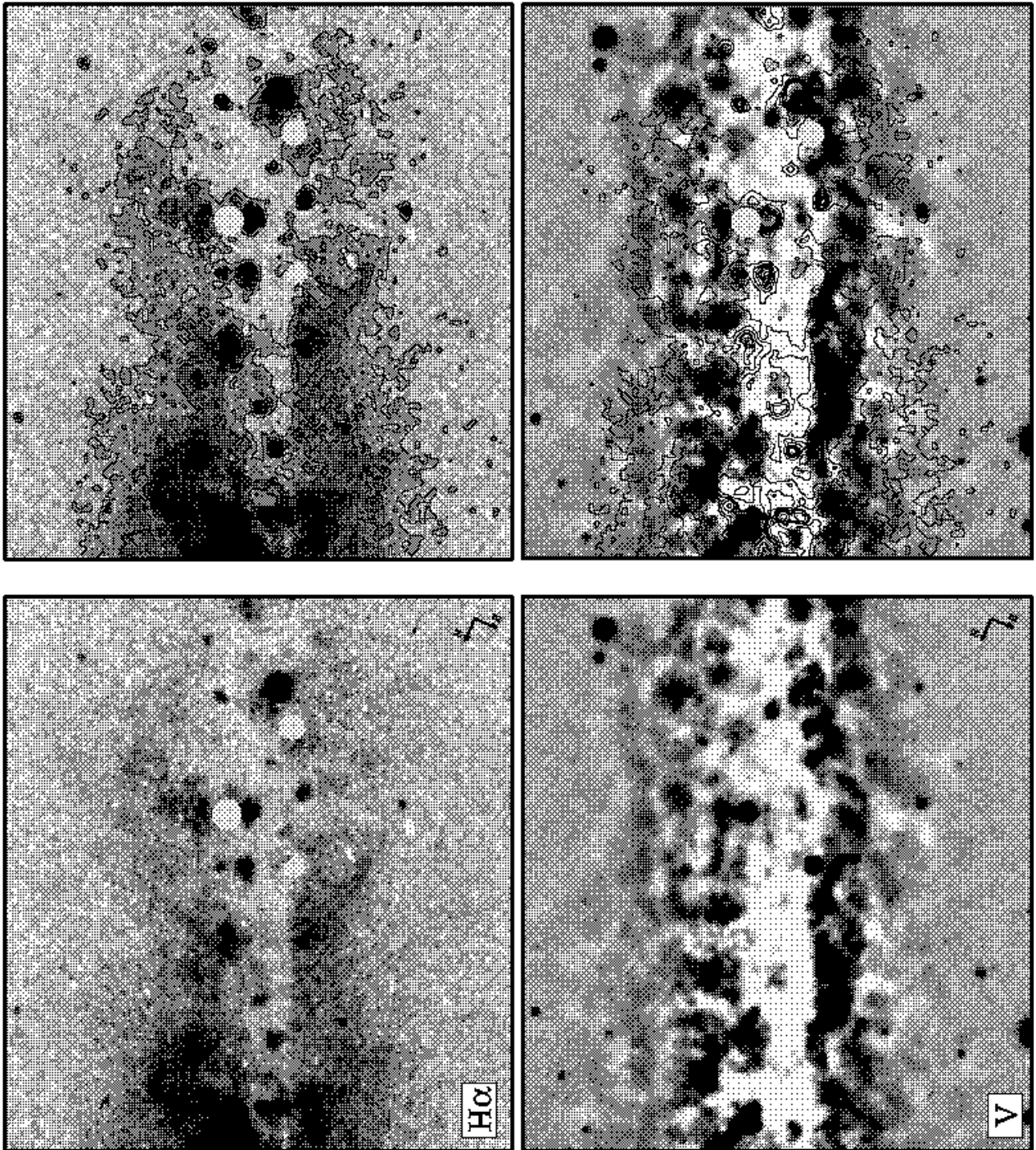


FIG. 13.— As Figure 11 but for a section of the disk centered ~ 4.4 kpc southwest of the nucleus of NGC 891.

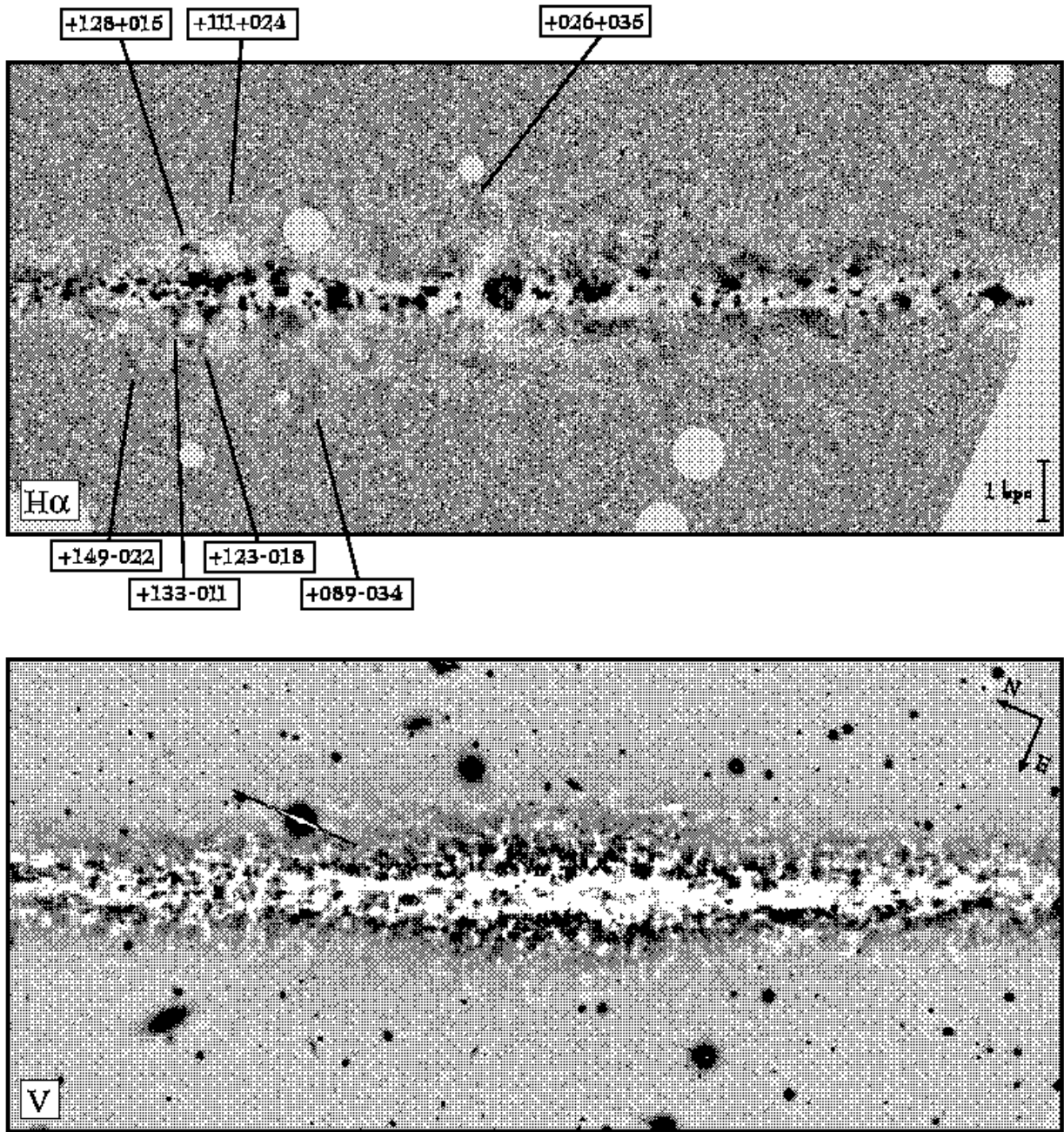


FIG. 14.— Unsharp masked views of both the continuum-subtracted $H\alpha$ emission line image of NGC 891 (top) and the V-band image (bottom). This image covers $6'.4 \times 2'.8$ ($17.3 \text{ kpc} \times 7.6 \text{ kpc}$). North and east are marked, and a 1 kpc scale bar is shown in the lower right portion of the $H\alpha$ image. The unsharp masked images (in both bands) were produced by dividing the original images by the images smoothed with a Gaussian kernel with $\text{FWHM} = 35$ pixels ($6''.9$). Several individual DIG filaments are identified in the upper panel. The properties of these structures are summarized in Table 4. It is clear from these images that there is significantly less structure in the $H\alpha$ images, which trace the DIG, than in the V-band images, which trace the dust absorption.